# Stepwise requirements for Polymerases δ and θ in Theta-mediated end joining

**Dale Ramsden** ( dale_ramsden@med.unc.edu )
UNC Chapel Hill https://orcid.org/0000-0003-1575-4748
**Susanna Stroik**
University of North Carolina at Chapel Hill
**Juan Carvajal-Garcia**
UNC Chapel Hill https://orcid.org/0000-0001-7257-3674
**Dipika Gupta**
New York University School of Medicine https://orcid.org/0000-0002-6512-5256
**Adam Luthman**
UNC
**David Wyatt**
UNC
**Wanjuan Feng**
University of North Carolina at Chapel Hill
**Thomas Kunkel**
National Institute of Environmental Health Sciences https://orcid.org/0000-0002-9900-1788
**Gaorav Gupta**
University of North Carolina at Chapel Hill https://orcid.org/0000-0001-9177-552X
**Eli Rothenberg**
New York University School of Medicine https://orcid.org/0000-0002-1382-1380

**Biological Sciences - Article**

**Keywords:**

**Posted Date:** September 19th, 2022

**DOI:** https://doi.org/10.21203/rs.3.rs-2057977/v1

# Stepwise requirements for Polymerases δ and θ in Theta-mediated end joining

Susanna Stroik[1], Juan Carvajal-Garcia[2], Dipika Gupta[3], Adam Luthman[4], David W. Wyatt[1,5], Wanjuan Feng[1], Thomas A Kunkel[6], Gaorav P. Gupta[1,4,7], Eli Rothenberg[3], Dale A Ramsden[1,4,5]

[1]Lineberger Comprehensive Cancer Center, University of North Carolina at Chapel Hill, Chapel Hill, NC, USA.
[2]Department of Biochemistry, Vanderbilt University, Nashville, TN, USA.
[3]Department of Biochemistry and Molecular Pharmacology, New York University School of Medicine, New York, NY, USA
[4]Department of Biochemistry and Biophysics, University of North Carolina at Chapel Hill, Chapel Hill, NC, USA.
[5]Curriculum in Genetics and Molecular Biology, University of North Carolina at Chapel Hill, Chapel Hill, NC, USA.
[6]Genome Integrity and Structural Biology Laboratory, National Institute of Environmental Health Sciences, National Institutes of Health, Research Triangle Park, North Carolina, USA
[7]Department of Radiation Oncology, University of North Carolina at Chapel Hill, Chapel Hill, NC, USA

## Summary Paragraph

Timely repair of chromosomal double strand breaks is required for genome integrity and cellular viability. The Polymerase Theta-mediated End Joining pathway has an important role in resolving these breaks and is essential in cancers defective in other DNA repair pathways, thus is an emerging therapeutic target[1] . It requires annealing of 2-6 nucleotides of complementary sequence – microhomologies – that are adjacent to the broken ends, followed by initiation of end-bridging DNA synthesis by Polymerase theta. However, the other pathway steps remain inadequately defined, and the enzymes required for them are unknown. Here we demonstrate additional requirements for exonucleolytic digestion of unpaired 3' tails before Polymerase theta can initiate synthesis, then a switch to a more accurate, processive, and strand-displacing polymerase to complete repair. We show the replicative polymerase, Polymerase delta, is required for both steps; its 3' to 5' exonuclease activity for flap trimming, then its polymerase activity for extension and completion of repair. The enzymatic steps that are essential and specific to this pathway are mediated by two separate, sequential engagements of the two polymerases. We show the requisite coupling of these steps together is facilitated by physical association of the two polymerases. This pairing of Polymerase Delta with a polymerase capable of end-bridging synthesis, Polymerase theta, may explain why the normally high-fidelity Polymerase delta participates in genome de-stabilizing processes like mitotic DNA synthesis[2] and microhomology-mediated break induced replication[3].

## Characterization of steps required for repair by theta-mediated end joining

Chromosome double strand breaks (DSBs) are repaired by Homologous recombination (HR), Nonhomologous end joining (NHEJ), or a poorly understood pathway dependent on Polymerase theta (Pol θ, gene name POLQ) appropriately termed theta-mediated end joining (TMEJ) [1]. In mammals, TMEJ is largely equivalent to microhomology-mediated end joining and alternative end joining. Initial pathway choice is determined in part by 5' to 3' nucleolytic resection of DSB ends, as the resulting 3' ssDNA tails are required for TMEJ and HR but impair repair by NHEJ. Genetic and biochemical studies argue TMEJ initiates by a Pol θ-dependent search to identify and anneal 2-6 nucleotides of complementary sequence on either side of the resected ends (Fig. 1a, Step 1)[4-6]. Pol θ is then essential for synthesis initiated from the annealed microhomology (MH). However, MHs of sufficient size for Pol θ to act are predicted to be embedded in 3' ssDNA tails for over 95% of DSBs[7], thus the resulting 3' flaps must first be trimmed by a previously uncharacterized nuclease before Pol θ can initiate synthesis. The steps following initiation of synthesis by Pol θ are also not well understood (Fig. 1a, after Step 3).

We investigate here the steps integral to the TMEJ pathway, as well as the enzymes required for each step. We initially employ a series of extrachromosomal substrates (Fig. 1a), which when introduced into mammalian cells require Pol θ for efficient repair (Fig. 1b, Extended data Fig. 3a; repair measured by qPCR is at least 100-fold lower in cells deficient in Pol θ, relative to the wildtype control).

We explored first the type of nuclease (i.e., endonuclease or exonuclease) responsible for removing 3' flaps (Fig. 1a, step 2). We used substrates wherein a 4 nucleotide MH is annealed to generate 5 nucleotide 3' flaps, then introduced nuclease-blocking phosphorothioate (PT) substitutions at varied phosphodiester bonds in the flaps. We assessed first the impact of PTs in the 4 bonds located closest to the 3' terminus of both ends, leaving only the bond that must be cleaved to activate synthesis (the 5$^{th}$ bond) unmodified. No significant TMEJ is observed when both ends were modified in this fashion (Fig. 1b). The nuclease required must thus cleave bonds downstream of the critical 5$^{th}$ phosphodiester, progressing to this bond in steps. Notably, there was no significant effect on repair of blocking only one end, arguing TMEJ does not require synthesis to be bi-directional. We then assessed effects of a single PT substitution on one end while blocking the other with 4 PT substitutions. We observed equivalent, 2-fold inhibition when comparing PT substitution of the most 3' terminal bond vs. the critical 5$^{th}$ bond (41% vs. 47%) (Fig. 1b). That repair is inhibited approximately 2-fold is consistent with the presence of two stereoisomers in PT substituted bonds, only one of which blocks nuclease activity[8]. We conclude flap trimming during TMEJ requires a ssDNA specific, 3' to 5' exonuclease (i.e., a nuclease that obligatorily cleaves in mononucleotide steps, starting from the 3' terminus).

We next investigated whether Pol θ-initiated synthesis from the trimmed end is sufficient to complete repair. We tracked Pol θ synthesis in repair products using its mutational signature - a tendency to insert or delete an adenine opposite 3 successive template thymidines that is much higher than other DNA polymerases[9]. We altered the extrachromosomal substrate described above to possess 3 thymidines every 5 nts in the template, then sequenced products of cellular repair, as well as a control reaction

assessing error due to sample processing (Fig. 1c). The Pol θ signature was evident at the first triple thymidine site only, suggesting Pol θ typically performs 6-14 nucleotides of DNA synthesis during TMEJ before there is a switch to a more accurate polymerase (Fig. 1d).

Synthesis in TMEJ may then arrest after gap filling and ligation, as in NHEJ, or it may continue and displace the downstream strand. We sought to distinguish between these resolving mechanisms by embedding a mispaired BamHI site in double stranded DNA, 20 or 50 bps downstream of the 5' end in our extrachromosomal substrate (Fig. 1e). This BamHI site remains mispaired if synthesis arrests after gap filling and ligation, as is apparent from the resistance of cellular NHEJ repair products to BamHI digestion (Fig. 1f). By comparison, TMEJ repair products are >90% sensitive to BamHI digestion when located 20 bp downstream, and 80% sensitive to BamHI digestion when located 50 bp downstream (Fig. 1f, Extended data fig. 1). Repair by NHEJ, but not TMEJ, is also impaired by a ligation-blocking abasic site at the 5' end of the downstream strand. We conclude TMEJ is resolved with strand-displacing synthesis, typically continuing in excess of 50 bp downstream.

**Polymerase Delta is required for both flap trimming and processive synthesis**

Our results indicate a 3' to 5' exonuclease trims flaps before Pol θ initiates synthesis and suggest there is a subsequent switch to synthesis mediated by a more accurate, processive, and strand-displacing polymerase. Polymerase delta (Pol δ) is a plausible candidate for performing both roles; its synthesis activity is sufficiently robust, but it is less clear whether its intrinsic 3'>5' exonuclease can effectively trim the flaps relevant to this pathway. We assessed this *in vitro*, using purified yeast Pol δ and DNA substrates mimicking the range of TMEJ intermediates expected in cells (2, 5 and 10 nucleotide flaps)[7]. We observe similarly robust and accurate trimming activity on all three substrates and confirmed this activity was missing in a Pol δ mutant specifically defective in its exonuclease activity (Fig. 2a). Moreover, sequential PT substitutions in flap phosphodiester bonds inhibit trimming activity of Pol δ by approximately 2-fold for each nucleotide step (Extended data fig. 2a), which is consistent with our cellular results (Fig. 1b).

We therefore depleted cells of active Pol δ using a lentiviral shRNA specific to the catalytic POLD1 subunit, then complemented these cells with either wild type Pol δ or mutants defective in either 3' to 5' exonuclease activity (D402A, $Exo^M$) or polymerase activity (S605del, $Pol^M$) (Fig. 2b, Extended data fig. 2b)[10,11]. We additionally designed two TMEJ substrates, each specifically dependent on one of the two steps; a flapped substrate dependent on trimming but requiring only minimal synthesis (Fig. 2c and Extended data fig. 2c; blue box), as well as a substrate that doesn't require trimming (unflapped) but dependent on processive synthesis (Fig 2d and Extended data fig. 2c; yellow box). To exclude possible non-specific effects of Pol δ depletion on pathway function, we compared repair of these substrates to a minimal TMEJ substrate (unflapped, requires minimal synthesis) (Extended data fig. 2c; grey box) that we included in electroporations as a spike-in control.

We show that repair requiring trimming of a 5 bp flap is negligible in cells deficient in endogenous Pol δ or $Exo^M$ expressing cells but is unaffected in cells expressing $Pol^M$ (Fig. 2c). Repair requiring trimming of 2 and 10 bp flaps has similar dependencies

(Extended data fig. 2d,e). Repair of the substrate requiring processive (70 nt) synthesis was similarly negligible in Pol δ deficient cells, but here we observed the expected reciprocal dependencies on Pol δ variants; TMEJ was negligible in cells expressing $Pol^M$, and unaffected for $Exo^M$ (Fig. 2d). An intermediate level of dependency on Pol δ is observed when repair requires 45 nt of synthesis (reduced 2-fold) (Extended data fig. 2f).

Next, we sought to assess the role of Pol δ in chromosomal TMEJ by introducing chromosome breaks at the LBR locus using Cas9. We quantified two MH-associated deletion products and a locally template dependent insertion product (TINS) expected to be dependent on TMEJ[7,12] , as well as an NHEJ-mediated 1 bp insertion product[13] (Fig. 3a, Extended data fig. 4a,b). The two MH-associated deletion products differ as to whether predicted MH alignments will be fully dependent on flap trimming, as one MH is embedded (flaps on both ends), while the other is terminal (a flap on only one end). Both products are significantly depleted in cells deficient in Pol θ, as expected. Importantly, both products are equally depleted in cells deficient in Pol δ, cells deficient in both Pol θ and Pol δ, as well as cells expressing $Pol^M$ (Fig. 3c,d). Cells expressing $Exo^M$ are also equally impaired in their ability to generate the embedded MH product (Fig. 3b). However, $Exo^M$ expressing cells have higher levels of the terminal MH product, consistent with a reduced requirement for exonuclease activity on the predicted intermediate (Fig. 3c). Both Pol δ activities are also required for TINS, a repair product that, though rare, is more specific to TMEJ (Fig. 3d). Pol δ depletion does not impair NHEJ, indicating effects are specific to TMEJ (Fig. 3e). We additionally do not observe similar effects on TMEJ upon depletion of Polymerase Epsilon, the leading strand replicative polymerase (Extended data fig. 4b-c). TMEJ thus requires Pol δ as much as it does Pol θ, engages resected intermediates that require at least 45 nt of synthesis for repair, and can dispense with the requirement for Pol δ exonuclease activity on rare occasions when MHs are present at the exact termini of resected ends.

**Polymerases Theta and Delta physically interact during cellular TMEJ**

We have shown TMEJ requires in sequence the alignment of MHs by Pol θ, flap trimming by Pol δ, initiation of synthesis by Pol θ, and finally switching to more processive synthesis mediated by Pol δ. This need for alternating engagements of the two polymerases on a common substrate is best served by a physical association. We therefore introduced a tagged Pol θ (Halo-Polq) into RPE1 cells and immunoprecipitated this protein. We recovered Pol δ, confirming the two polymerases physically interact (Fig. 4a). We then assessed if the two conserved domains of Pol θ – a Helicase-like domain and its Polymerase domain[1] – independently interact with Pol δ, by separately introducing flag tagged versions of each domain into Pol θ deficient U2OS cells. Both could be recovered after immunoprecipitating Pol δ, thus both independently associate with Pol δ (Fig. 4b). We sought to also address association of the two polymerases in intact cells by employing super resolution microscopy of Pol δ, Pol θ, and the DSB marker 53BP1 (Fig. 4c). We observed a damage-dependent increase in Pol δ density near Pol θ associated DSBs, indicating both polymerases engage the same DSB in intact cells (Fig. 4d).

## Discussion

We clarify here the remaining steps essential for TMEJ, as well as the enzymes required for them. We demonstrate there is an exonucleolytic trimming step required before Pol θ can initiate synthesis, and a switch to synthesis by a more processive and strand displacing polymerase (Fig. 1, 4e). Pol δ is required for both steps – with no evidence for redundancy (Fig. 2). TMEJ is also equally impaired by deficiencies in either polymerase alone, as well as combined deficiency, indicating Pol δ is just as essential to pathway function as is Pol θ (Figs. 2, 3). By comparison, Pol δ is important for alternative end joining in the fungus *S. cerevisiae*[14-16], but fungi have no counterpart to Pol θ[17]. The increased flexibility provided to TMEJ by Pol θ helps explain the more central role this pathway plays in DSB repair in all other eukaryotes.

Pol δ exonuclease activity is normally linked to editing of mispairs incorporated during replication[18], as well as a backup function in trimming 3' flaps during DSB repair by HR[19]. In both cases extensive upstream double stranded DNA (>15 bp) arrests trimming and cues the switch to Pol δ-mediated synthesis. Trimming by Pol δ during TMEJ critically differs in that the flapped intermediate possesses minimal upstream double stranded DNA (as little as 2 bp) and can persist only if MH annealing by Pol θ is maintained throughout the trimming process. We can thus infer that flap trimming by Pol δ during TMEJ is arrested via steric block by Pol θ at the annealed MH. We also expect the physical association observed between the two polymerases (Fig. 4) will be essential for the requisite coupling of MH alignment by Pol θ, to precise end trimming by Pol δ, to initiation of synthesis by Pol θ.

Pol θ alone is not sufficiently processive when TMEJ requires synthesis >70 nts, and only partly competent when TMEJ requires synthesis >45 nts (Fig.2d, Extended data fig. 2f). Pol δ synthesis activity is also notably required for TMEJ of the blunt DSBs generated by Cas9 in the chromosome (Fig. 3), indicating the DSB intermediates engaged by this pathway have ends resected in excess of 45 nucleotides. However, mutation spectra suggested switching from Pol θ to Pol δ occurs prior to 14 nt of synthesis (Fig. 1d). We suggest when both polymerases are present, Pol θ disengages much earlier than 45 nucleotides. Pol δ may simply have higher affinity for the primer once Pol θ sufficiently extends the 2-6 bp MH, i.e., there is in sum significantly more than 15 bp of upstream double stranded DNA. Alternatively, there may be a mechanism that actively drives switching, analogous to Rad18-promoted polymerase switching at stalled replication forks[20]. It will additionally be important to determine the extent synthesis by Pol δ during TMEJ relies on factors normally linked to activity of this polymerase during replication[21] – especially the PCNA processivity clamp – or whether Pol θ functionally substitutes for these factors.

A switch to synthesis mediated by Pol δ is likely also required for coordinating the steps required for final resolution. We show TMEJ is associated with strand displacing synthesis (Fig. 1f), and Pol θ appears less effective than Pol δ in this regard[22]. More importantly, the final steps of TMEJ involve 5' flap removal by Fen 1[23] and ligation by Ligase III and Ligase I[24-27], and there is precedent for coupling Pol δ-mediated strand displacement to these steps during both long-patch base excision repair[28] and Okazaki fragment resolution[29].

The pairing of Pol θ with the replicative polymerase Pol δ is consistent with emerging evidence arguing for an important role for Pol θ in response to replication

stress[30-35]. The pivotal roles TMEJ has – both in response to replication stress and during conventional DSB repair – rely on the flexibility provided by coupling Pol θ-mediated end-bridging synthesis to Pol δ. However, this flexibility may come at a cost. Pairing of a promiscuous Pol θ with the normally high-fidelity Pol δ may help explain the role of Pol δ in a variety of processes that generate large-scale genome rearrangements, including microhomology mediated break-induced replication (MMBIR), mitotic DNA synthesis (MiDAS), and translocation[2,3,35-37].

## Materials and Methods

### Cell lines

All cells were cultured in 5% $CO_2$ at 37°C and regularly tested and shown to be mycoplasma negative by PCR (detection limit less than 10 genomes/mL). Human embryonic kidney cells (HEK-293Ts), mouse embryonic fibroblasts transformed by SV40 T-antigen (MEFs), and POLQ$^{-/-}$ human bone osteosarcoma epithelial cells (U2OS) were cultured in DMEM media (Corning). Human colon carcinoma cells (HCT116s) were cultured in McCoy's media (Corning). P53$^{-/-}$ retinal pigment epithelial cells (RPE1s) immortalized by human telomerase reverse transcriptase were cultured in DMEM-F12 (Invitrogen). All media was supplemented with 10% Fetal Bovine Serum (VWR, Seradigm) and penicillin (5U/mL, Sigma). RPE1 P53$^{-/-}$ POLQ$^{-/-}$ and Halo-tagged POLQ cell lines were generous gifts from the lab of Dr. Gaorav Gupta and previously described[38]. U2OS POLQ$^{-/-}$ cells were a generous gift from Dr. Rick Wood and have been previously described[39].

### Generation of recombinant cell lines

For POLD1 and POLE knockdown, lentiviral constructs (Addgene 160792, 160762) were transfected with lentiviral packaging constructs (Addgene 12260, 12259) into HEK-293T cells using Transporter 5 (Polysciences). For POLD1 cDNA expression, retroviral constructs were transfected (Addgene 160805) with retrovirus packaging constructs (Addgene 35616, 14887) in the same manner described above. Mutant retroviral cDNA constructs were generated using Q5 mutagenesis (NEB) of the WT cDNA plasmid and validated by sanger sequencing. Media was changed 18-24 hours post-transfection, and virus was collected at 48 and 72 hours post transfection. Cells to be transduced were plated 1 day prior to the first viral harvest. Viral-containing media from the HEK-293Ts was filtered through a 0.45 um filter and supplemented with 1 ug/ml polybrene prior to transduction via media change of the target cells. Cells were serially transduced with both the 48 and 72 hour viral media collections from the HEK-293Ts. The day after the second transduction, cells were plated into media containing either blasticidin or puromyocin selection for 2 days. The media was changed and cells were allowed to recover for 1 day prior to experimental use or freezing down at -80 C°. All plasmids used to generate recombinant lines were validated and sequenced at Plasmidsaurus. Where shPOLD1 or shPOLE were used in RPE1 cells, RPE1 PAC$^{-/-}$ cells were used and untreated RPE1 PAC$^{-/-}$ cells were used as parental controls (wt).

### Extrachromosomal assays

All extra chromosomal substrates except for those detailed in Fig. 1f and Extended data fig. 1 were annealed from Ultramer DNA (IDT) in a thermocycler with a 5 minute 95 °C denaturation, 1 hour at 70 °C, and finally cooled to 4 °C with a 0.5% cooldown rate between steps. DNA was annealed in 10 mM Tris pH 7.5, 100 mM NaCl, and 0.1 mM EDTA buffer. 500 ng of the TMEJ substrates and 20 ng of the NHEJ substrate were electroporated into 250,000 cells with a dual 1,350 volt, 20 ms pulse with the Neon system (Invitrogen). Where indicated, cells were pre-treated for 2 hours with 2 uM ART558 (Artios Pharma) prior to electroporation and were recovered for 30 minutes post-electroporation in media or drug-supplemented media. Cells were then washed in PBS and incubated in Hank's balanced saline solution containing 25U of Benzonase (Sigma) for 15 minutes. DNA extraction was then performed using the QIAamp DNA mini kit (Qiagen) and samples were subsequently analyzed via PCR using the TaqMan Fast Advanced Master Mix (Applied Biosystems; relevant primers and probes described in supplemental table 2). PCR efficiency, limit of detection (LOD), and independence of multiplex PCRs for all qPCR amplicons was determined by serially diluting a synthetically produced model amplicon product into genomic DNA containing a constant amount of the relevant reference amplicon for that target (Extended data fig. 3). The inverse of this quality check was also performed on each target/reference pair. All model amplicon products are detailed in Supplementary Table 5. In extrachromosomal substrate experiments, TMEJ activities were normalized to repair measured with spike-in control substrates (Table 1), either NHEJ (Figure 1b) or minimal TMEJ substrates (Figure 2, Extended Data 2), in a multiplexed reaction, as indicated in respective figures. All experiments consisted of 3 replicates of each electroporation. Ultramer DNA oligos and qPCR primer and probe pairs are described in Supplementary Tables 1 and 2, respectively.

Substrates employed in experiments described in Fig. 1f were assembled by golden gate ligation of left and right annealed oligonucleotide dsDNA ends to a 600 bp central DNA fragment as described[7] using the oligonucleotides described below. These substrates were introduced into mouse embryo fibroblasts as described[7]. Recovered DNA was mock digested or digested with BamHI when indicated, amplified, and electrophoresed on native 6% polyacrylamide gels to identify overhang-containing products.

**Immunoblotting**

Whole cell lysates were prepared with radioimmunoprecipitation assay (RIPA) buffer supplemented with a freshly prepared protease inhibitor cocktail (Sigma, P8340). Lysates were denatured in Laemmli sample buffer (Biorad, 1610737) and loaded onto 5-15% tris-glycine SDS polyacrylamide gels. Protein was transferred to nitrocellulose membranes in a 20% methanol supplemented tris-glycine transfer buffer. Membranes were blocked in TBST containing 3% BSA for 1 hour at room temperature. Primary antibodies were diluted in blocking buffer and incubated with membranes overnight with agitation at the following dilutions (POLD1 (Abcam, 186406) 1:2,000; Actin (Novus, NB600-535) 1:10,000; HALO (Promega, G9211) 1:1,000; POLE (GeneTex, GTX132100) 1:2,000; FLAG (Sigma, F3165) 1:2,000). Membranes were washed with TBST and incubated with appropriate secondary antibodies (Licor) at a dilution of 1:7,000 in blocking buffer for 1.5 hours at room temperature. Membranes were imaged

and analyzed on a Licor Odessey machine. All uncropped blots are available in Extended data fig. 5.

**Co-IP**

Where indicated, cells were pre-treated with Neocarzinostain (Sigma) at 100 ng/mL for 2 hours prior to lysate collection. Lysates were prepared in a non-denaturing buffer (25 mM Tris, 150 mM NaCl, 1 mM EDTA, 1% NP-40) supplemented with freshly prepared protease inhibitor cocktail. Magnetic beads (BioRad, 1614013) were incubated with 7 ug of the appropriate antibody for 20 minutes at room temperature. Beads were then washed 3 times with PBST and incubated at 4°C with prepared lysates for 6 hours with gentle agitation. Beads were washed 3 times and proteins were boiled and eluted into Laemmli sample buffer. Lysates were treated with benzonase to eliminate DNA in the protein samples. 5% input and IP elutions were subsequently processed with the previously described immunoblotting protocol.

**In vitro assays**

Olignucleotides for exonuclease substrates were purchased from IDT and annealed. Wild type and exonuclease defective (D520V) *S. cer.* Pol δ were the gift of Dr. Tom Kunkel, and purified as described[40]. 5' Cy5 labeled double stranded DNA substrates with 2,5, or 10 nt 3' ssDNA overhangs were incubated with purified wild type (wt) or exonuclease defective (D520V) Pol δ for 1 (wild type) or 5 minutes (Exo mutant) at 37ºC. Reactions were performed in a buffer containing 25mM TRIS ph8.0, 135mM KCl, 5mM $MgCl_2$, and 100 µM each of all 4 dNTPs and stopped after the indicated time by addition of an equal volume of formamide and 10mM EDTA. Samples were then heated for 5 minutes at 95ºC, separated on a 5% polyacrylamide gel under denaturing conditions, and imaged using a Typhoon FLA9500 to detect a 5' terminal Cy5 label. All uncropped gels are available in Extended data fig. 5.

**Next-generation sequencing of polymerase theta products**

Cellular transfection and DNA extraction were carried out as described in the extrachromosomal assays. Desalted DNA primers (IDT) were used to amplify the repair product of interest for 25 PCR cycles. PCR products were purified via gel extraction from a 2% agarose (Lonza) gel and the QIAquick Gel Extraction Kit (Qiagen). DNA Ultramers (IDT) containing a substrate-specific primer sequence, 6 bp barcode, spacer sequence of varying length, and Illumina's adapter sequences were used to perform a secondary amplification for 7 PCR cycles. These PCR products were further purified with AMPure Magnetic beads (Beckman). Final DNA libraries were sequenced with an Illumina Iseq 100 i2 kit (300 cycles) with a 15% PhiX Control DNA spike-in (Illumina). Ultramer oligos and primer pairs are described in Supplementary Table 3.

Sequencing data was trimmed, and reads were merged using CLC Genomic Workbench 8 (Qiagen). Triplet thymidine location was identified according to 5 nt unique barcodes both upstream and downstream of the triplet thymidines (5'-nnnnnTTTnnnnn-3'). Polymerase theta errors at triplet repeats (TTT) predominantly manifest as slippage resulting in 1 nucleotide insertions (TTTT) or deletions (TT). Thus, we modeled each of these outcomes and counted the frequency of indels (+1 or -1 nt) at each triplet, moving proximal to distal away from the MH. Reads were excluded wherein the 5 nt barcodes

contained deletions, insertions, or substitutions, thus limiting our analysis to errors in the repeat regions. Analysis of samples was performed in Microsoft Excel.

**Cas9 chromosomal reporter assay**

The CRISPR RNA (crRNA) specific to a site in the human LBR gene is described in Supplementary Table 4. To generate a DSB at the LBR locus, 7 pmols of Cas9 was incubated with 8.4 pmols of crRNA annealed to tracRNA (IDT, Alt-R) for 30 minutes at room temperature. This complex was electroporated into 250,000 cells as described above. Two electroporations were pooled together to comprise a single biological replicate. Cells were then re-plated into the previously indicated media for 48 hours. DNA was harvested from cells using the QIAamp DNA mini kit (Qiagen). Repair products were quantified with qPCR using 50 ng of input DNA and the TaqMan Fast Advanced Master Mix (Applied Biosystems). Relevant primers and probes are described in supplementary table 2. All signature PCRs (TMEJ/NHEJ) were normalized to a reference amplicon 10 kb upstream of the Cas9-cut site multiplexed in the same reaction. PCR efficiencies and LODs for this assay were determined by diluting a Cas9-treated WT cell line sample into unbroken genomic DNA (Extended data fig. 3).

A custom Python script was developed to predict outcomes of theta-mediated end joining at unique genomic loci (PyCharm Community Edition 2021, JetBrains). In brief, we predict resolutions, both microhomology-mediated deletions and locally templated insertions (TINS), such that microhomologies are within 15 nucleotides and template for TINs is within 25 nucleotides, of the DSB[7].

**Droplet digital PCR**

Chromosomal DSBs were introduced via the Cas9 system described above at the LBR locus. Droplet digital PCR was performed with 100 ng of genomic DNA and ddPCR Supermix for Probes (no dUTP)(BioRad). The TINS signature amplicon information is described in Supplemental Table 2 and the reference amplicon was the same as previously described in the qPCR assay. Droplets were generated and read using a QX200 AutoDG Droplet Digital PCR system. QuantaSoft software was used to analyze resulting data.

**Super resolution imaging and analysis**

Cells were seeded onto glass coverslips (Fisher Scientific, 12-548-B) 1 day prior to experimentation. Cells were incubated with Neocarzinostain (Sigma) at 40 ng/mL for 2 hours prior to harvest, 10 uM EdU for 30 minutes, and Janelia Fluor 646 (Promega, GA1120) at 1 ng/uL for 30 minutes. Cells were then permeabilized with 0.5% Triton X-100 in ice-cold CSK buffer (10 mM Hepes, 300 mM Sucrose, 100 mM NaCl, 3 mM $MgCl_2$) for 3 minutes followed by 3 PBS washes. Cells were then fixed with 4% paraformaldehyde (EMS, 15714) for 15 minutes. Coverslips were subsequently washed twice with PBS and blocking buffer (2% glycine, 2% BSA, 0.2% gelatine, 50 mM $NH_4Cl$) 3 times. Cells were incubated in blocking buffer overnight at 4 °C. Click reactions were then performed on coverslips to label EdU and coverslips were subsequently washed 3 times. Coverslips were then incubated with primary antibody for 1 hour at room temperature (POLD1 abcam 186407, 1:250 dilution; 53BP1 Novus NB100-304, 1:10,000). After blocking buffer washes, coverslips were incubated with secondary

antibodies in blocking buffer (Invitrogen, AF488 and AF568 both at 1:10,000). Coverslips were then washed thrice with blocking buffer and mounted onto glass slides with freshly prepared imaging buffer (1 mg/ml glucose oxidase (Sigma, G2133), 0.02 mg/ml catalase (Sigma, C3155), 10% glucose (Sigma G8270), 100 mM mercaptoethylamine (Fisher Scientific, BP2664100)) flowed through prior to imaging.

For single molecule localization microscopy imaging, image stacks with at least 2000 frames per channel, acquired at 33 Hz, were taken on a custom-built optical imaging platform based on a Leica DMI 300 inverted microscope possessing three laser lines 561 nm (Coherent, Sapphire 561 LPX-500), 639 nm (Ultralaser, MRL-FN-639-1.2), and 750 nm (UltraLaser, MDL-III-750-500). Lasers were combined and aligned using dichroic mirrors and were focused on the back aperature of an oil immersion objective (Olympus, IApo N, 100x, NA=1.49, TIRF) with a multiband dichroic mirror (Semrock, 408/504/581/667/762-Di01). Fluorophores were individually excited with a Highly Inclined and Laminated Optical (HILO) illumination configuration. Emissions were expanded with a 2X lens tube and filtered using single-band pass filters in a filter wheel (ThorLabs, FW102C) and collected on a sCOMS cameras (Photometrics, Prime 95B). A 405 nm laser line (MDL-III-405-150, CNI) was used with AF647 to drive it back to its ground state. Images were acquired using Micro-Manager (v2.0) software.

Localization of each single molecule was performed as previously described in[41-44]. Representative images were generated by rendering raw coordinates onto a 10 nm pixel canvas, convolved with a 2D-Gaussian ($\sigma$ = 10 nm) kernel, and adjustment of individual channel brightness for display purposes. Result tables with the localization coordinates of each individual fluorophore blinking within a 6 x 6 $\mu m^2$ region of interest (ROI) underwent Auto-Pair-Correlation analyses[45,46] to estimate the density of each fluorophore. Artificial and artifactual blinking events were removed before the computation of cross-pair correlations. A correlation profile was generated as a function of the pair-wise distances and fit to a Gaussian model. Average molecular content and the density within a focus was derived based on the computed average probability of finding a particular species around itself and the apparent average radius of the focus. This functionally estimated the nuclear density of POLQ, 53BP1, and POLD1 fluorophores within a nucleus in addition to the average number of fluorophores within each focus. For Cross-PC analyses, correlation profiles were plotted as a function of the pairwise distance between POLQ and POLD1 and fitted it to a Gaussian model to determine the cross POLQ-POLD1 pair correlation amplitude. With this analysis, we estimated the average local density of POLD1 around each POLQ molecule localized to a 53BP1 within a given ROI.

**Statistical analysis**

All replicate numbers and statistical tests performed are listed with their corresponding figures.

All statistical analysis was carried out using GraphPad Prism 9. Statistical significance is displayed in figures as *,**,***,*** represents $p \leq .05, .01, .001, .0001$, respectively. Statistical tests for qPCR experiments were run on cycle thresholds prior to transformation of data for the linear scale representations shown in display figures. p

values were adjusted using Dunnet's method to correct for multi comparisons when more than two groups were compared.

## Software

Model figures were made using BioRender and Adobe Illustrator. Graphs were generated in GraphPad Prism.

## Author Contributions

Generated and analyzed data or developed methodology or reagents: all authors. Initial draft of the manuscript: S.J.S and D.A.R. Editing of the manuscript and final drafting: all authors. Conceptualization of the study: S.J.S and D.A.R.

## Competing Interests

D.A.R has a materials transfer agreement with Artios Pharma and is using an Artios Pharma compound for research purposes with no financial compensation.


## Acknowledgements

We would like to thank Artios Pharma Limited for supplying ART558, Drs. Rick Wood and Kei-ichi Takata for supplying U2OS POLQ$^{-/-}$ cells and generating the Halo-Polq plasmid. D.A.R is funded by 1P01CA247773 and 5U01CA097096. SJS is supported by F32CA264891 and T32CA009156.


## Supplementary Table 1: DNA Extrachromosomal substrate sequences

| Substrate | Orientation | Sequence |
|---|---|---|
| TMEJ phosph-othioate blocked | Top | cgacctttttggtcgttttctcacacccatcgtacatcattcgtctctatggacccggcagtgg gatcctgacgctgaggttacggcagtgcgtgagttcggtatagtatggtactaagcgatgc tctcaccgagggatggcagt*t*t*t*t |
| TMEJ no flap | Bottom | cgacctttttggtcgtttgcatcgcttagtaccatactataccgaactcacgcactgccgtaa cctcagcgtcaggatcccactgccgggtccatagagacgaatgatgtacgatgggtgtg agagtgaagatcctcaccttcggagtactccttcttttgaccatcgatcgtgataggacata cagctctgc |
| TMEJ 2 BP flap | Bottom | cgacctttttggtcgtttgcatcgcttagtaccatactataccgaactcacgcactgccgtaa cctcagcgtcaggatcccactgccgggtccatagagacgaatgatgtacgatgggtgtg agagtgaagatcctcaccttcggagtactccttcttttgaccattgatacgatacttctcagcc gagctgctt |
| TMEJ 5 BP flap | Bottom | cgacctttttggtcgtttgcatcgcttagtaccatactataccgaactcacgcactgccgtaa cctcagcgtcaggatcccactgccgggtccatagagacgaatgatgtacgatgggtgtg agagtgaagatcctcaccttcggagtactccttcttttgaccattgatacgatacttctcagcc gagctgcttttt |
| TMEJ 10 BP flap | Bottom | cgacctttttggtcgtttgcatcgcttagtaccatactataccgaactcacgcactgccgtaa cctcagcgtcaggatcccactgccgggtccatagagacgaatgatgtacgatgggtgtg |

| | | |
|---|---|---|
| | | agagtgaagatcctcaccttcggagtactccttctgaccattgatacgatacttctcagccg agctgctttttttttt |
| TMEJ 25 BP synthesis | Top | cgacctttttggtcgttttctcacacccatcgtacatcattcgtctctatggacccggcagtgg gatcctgacgctgaggttacggcagtgcgtgagttcggtatagtatggtactaagcgatgc tctcaccgagggccttgccagcagt*t*t*t*t*t |
| TMEJ 45 BP synthesis | Top | cgacctttttggtcgttttctcacacccatcgtacatcattcgtctctatggacccggcagtgg gatcctgacgctgaggttacggcagtgcgtgagttcggtatagtatggtactaagcgatgc tctcaccgagggacgtatctgctgggttgtggataccgaggcagt*t*t*t*t*t |
| TMEJ 70 BP synthesis | Top | cgacctttttggtcgttttctcacacccatcgtacatcattcgtctctatggacccggcagtgg gatcctgacgctgaggttacggcagtgcgtgagttcggtatagtatggtactaagcgatgc tctcaccgagggacgtatctgctgggttgtggatgaattcatgctgtgggttgtggatcgagt aggcagt*t*t*t*t*t |
| TMEJ phospho-rothioate blocked | Bottom | cgacctttttggtcgtttgcatcgcttagtaccatactataccgaactcacgcactgccgtaa cctcagcgtcaggatcccactgccgggtccatagagacgaatgatgtacgatgggtgtg agagtgaagatcctcaccttcggagtactccttctttttgaccattgatacgatacttctcagcc gagctgct*t*t*t*t*t |
| TMEJ terminal phospho-rothioate blocked | Bottom | cgacctttttggtcgtttgcatcgcttagtaccatactataccgaactcacgcactgccgtaa cctcagcgtcaggatcccactgccgggtccatagagacgaatgatgtacgatgggtgtg agagtgaagatcctcaccttcggagtactccttctttttgaccattgatacgatacttctcagcc gagctgctttt*t |
| TMEJ branch point phospho-rothioate blocked | Bottom | cgacctttttggtcgtttgcatcgcttagtaccatactataccgaactcacgcactgccgtaa cctcagcgtcaggatcccactgccgggtccatagagacgaatgatgtacgatgggtgtg agagtgaagatcctcaccttcggagtactccttctttttgaccattgatacgatacttctcagcc gagctgc*ttttt |
| TMEJ 5 BP flap | Top | cgacctttttggtcgttttctcacacccatcgtacatcattcgtctctatggacccggcagtgg gatcctgacgctgaggttacggcagtgcgtgagttcggtatagtatggtactaagcgatgc tctcaccgagccgtatctgctgggttgtggatgaattacatatgctgggagaaccaagattg ggcagttttt |
| NHEJ | Top | gacaccttagctgtatagtcaccctgcagaactatcgaatagcacgattcactctgttccat gatcttcactctcacacccatcagcagtgggacttcggctgaggaggacactgctgttaga cttgtggtggatgacctaagcgatgctctcaccgaggattatcgagcaagaagcagggta gccagtctgagaatcga |
| NHEJ | Bottom | gattctcagactggctaccctgcttcttgctcgataatcctcggtgagagcatcgcttaggtc atccaccacaagtctaacagcagtgtcctcctcagccgaagtcccactgctgatgggtgt gagagtgaagatcatggaacagagtgaatcgtgctattcgatagttctgcagggtgactat acagctaaggtgtcga |

| | | |
|---|---|---|
| TMEJ TTT walking | Top | cgacctttttggtcgtttgcatcgcttagtaccatactataccgaactcacgcactgccgtaacctcagcgtcaggatcccactgccgggtccatagagacgaatgatgtacgatgggtgtgagagtgaagatcctttgctgatttactactttgatactttatatgtttgcgagtttctatgtttagtatgcagt*t*t*t*t |
| TMEJ TTT walking | Bottom | cgacctttttggtcgttttctcacacccatcgtacatcattcgtctctatggacccggcagtggatcctgacgctgaggttacggcagtgcgtgagttcggtatagtatggtactaagcgatgctctcaccgagctcaccttcggagtactccttcttttgaccattgatacgatgcttctcagccgagatctgc |
| TMEJ TTT walking control adapter | V1 | taagcgatgctctcaccgagctcaccttcggagtactccttcttttgaccattgatacgatgcttctcagccgagataaaaactgc |
| Strand displacement TMEJ | Top left, 20 bp BamHI | tgactatacagggatccacttctaagcgatgctctcaccgagcgtatctgctgtgttgtggatgaattagatgcag |
| Strand displacement NHEJ | Top left, 20 bp BamHI | tgactatacagggatccacttctaagcgatggacg |
| Strand displacement TMEJ | Bottom left, 20 bp BamHI | catcgcttagaagtcggaacctgtata |
| Strand displacement | Bottom left, 20 bp BamHI | (Furan)atcgcttagaagtcggaacctgtata |
| Strand displacement TMEJ | Bottom right, 20 bp away | agtctgagatgggatccacttggtgtgagagtgaagatcctcaccttcggagtactccttctttttgagatctg |
| Strand displacement NHEJ | Bottom right, 20 bp BamHI | agtctgagatgggatccacttggtgtgaggacg |
| Strand displacement | Top right, 20 bp BamHI | ctcacaccaagtcggaaccatctca |
| Strand displacement | Top right, 20 bp BamHI | (Furan)tcacaccaagtcggaaccatctca |
| Strand displacement | Top left, 50 bp BamHI | tgactatacagggatccacttctaagcgatgccatctcatccctgcgtgtctccgctctcaccgagcgtatctgctgtgttgtggatgaattagatgcag |
| Strand displacement | Bottom left, 50 bp BamHI | cggagacacgcagggatgagatggcatcgcttagaagtcggaacctgtata |

| | | |
|---|---|---|
| Strand displacement | Bottom right, 50 bp BamHI | agtctgagatgggatccacttggtgtgagcttggacaagtcgactggtcttaaggagtgaa gatcctcaccttcggagtactccttcttttgagatctgc |
| Strand displacement | Top, right, 50 bp BamHI | ccttaagaccagtcgacttgtccaagctcacaccaagtcggaaccatctca |

*represent phosphorothioate at denoted position

**Supplementary Table 2: qPCR amplicon information**

| Amplicon | Primer | Sequence |
|---|---|---|
| EC TMEJ no flap | Fwd | taagcgatgctctcaccga |
| | Rev | gatgggtgtgagagtgaagatc |
| | Probe | /56-fam/cgatcgtga/zen/taggacatacagctctgc/3iabkfq/ |
| EC TMEJ any flap | Fwd | taagcgatgctctcaccga |
| | Rev | gatgggtgtgagagtgaagatc |
| | Probe | /5hex/acgatactt/zen/ctcagccgagctgc/3iabkfq/ |
| EC TMEJ 25 BP synthesis | Fwd | taagcgatgctctcaccga |
| | Rev | gatgggtgtgagagtgaagatc |
| | Probe | /5hex/ccttgccag/zen/cagagctgtatgtcc/3iabkfq/ |
| EC TMEJ 45-70 BP synthesis | Fwd | taagcgatgctctcaccga |
| | Rev | gatgggtgtgagagtgaagatc |
| | Probe | /56-fam/tcgagtagg/zen/cagagctgtatgtcc/3iabkfq/ |
| EC NHEJ | Fwd | taagcgatgctctcaccga |
| | Rev | gatgggtgtgagagtgaagatc |
| | Probe | /56-fam/tctcagact/zen/ggctaccctgcttct/3iabkfq/ |
| TMEJ embedded LBR locus | Fwd | cagtgaacacctctgcataaa |
| | Rev | gagaagagagaaggagggtaca |
| | Probe | /56-fam/taggcaaagc/zen/tggatgttgtcacct/3iabkfq/ |
| NHEJ LBR locus | Fwd | gaacacctctgcatgaggc |
| | Rev | gagaagagagaaggagggtaca |
| | Probe | /56-fam/taggcaaagc/zen/tggatgttgtcacct/3iabkfq/ |
| Reference LBR locus | Fwd | Caaaacagagcaggggagaga |
| | Rev | Gcctttgcctggagaacttac |
| | Probe | /5hex/atggaggtg/zen/aagatgcaggtgtca/3iabkfq/ |
| TMEJ terminal LBR locus | Fwd | tgaacacctctgcatgagg |
| | Rev | gagaagagagaaggagggtaca |
| | Probe | /56-fam/taggcaaagc/zen/tggatgttgtcacct/3iabkfq/ |
| TMEJ TINS LBR locus | Fwd | tgaacacctcatgcagagg |
| | Rev | gagaagagagaaggagggtaca |
| | Probe | /56-fam/taggcaaagc/zen/tggatgttgtcacct/3iabkfq/ |

**Supplementary table 3: NGS primer details**

| Background | PCR order | Orientation | Sequence |
|---|---|---|---|

| | | | |
|---|---|---|---|
| All backgrounds | primary | Fwd | taagcgatgctctcaccga |
| | primary | Rev | gatgggtgtgagagtgaagatc |
| RPE1 WT | secondary | Fwd | aatgatacggcgaccaccgagatctacacactctttccctac acgacgctcttccgatctactgcataagcgatgctctcaccga |
| RPE1 WT | secondary | Rev | caagcagaagacggcatacgagatgtgactggagttcagac gtgtgctcttccgatcttcgcctgatgggtgtgagagtgaagatc |
| Q5 control | secondary | Fwd | aatgatacggcgaccaccgagatctacacactctttccctac acgacgctcttccgatctactgcataagcgatgctctcaccga |
| | secondary | Rev | caagcagaagacggcatacgagatgtgactggagttcagac gtgtgctcttccgatctgatactacgatgggtgtgagagtgaaga tc |

**Supplementary table 4: gRNA details**

| Locus | gRNA sequence + PAM | Location |
|---|---|---|
| LBR | gaacacctctgcatgagcagggg | Chr. 1 |

**Supplementary table 5: *In vitro* oligo details**

| Substrate | Sequence |
|---|---|
| **Bottom** | gcagctcggctgagaagtat |
| **Top, 2 nt flap** | /5cy5/atacttctcagccgagctgctt |
| **Top, 5 nt flap** | /5cy5/atacttctcagccgagctgcttttt |
| **Top, 10 nt flap** | /5cy5/atacttctcagccgagctgctttttttttt |
| **Top, 5 nt flap with 3 terminal phosphorothioates** | /5cy5/atacttctcagccgagctgctt*t*t*t |

**Supplementary table 6: Control model product sequences**

| Product | Sequence |
|---|---|
| Flapped TMEJ substrate | ctaagcgatgctctcaccgagggatggcagctcggctgagaagtatcgtatcaatggtcaaaag aaggagtactccgaaggtgaggatcttcactctcacacccatc |
| Unflapped TMEJ substrate | ctaagcgatgctctcaccgagggatggcagagctgtatgtcctatcacgatcgatggtcaaaaga aggagtactccgaaggtgaggatcttcactctcacacccatc |
| 25 bp TMEJ synthesis substrate | taagcgatgctctcaccgagggccttgccagcagagctgtatgtcctatcacgatcgatggtcaaa agaaggagtactccgaaggtgaggatcttcactctcacacccatc |
| 45 bp TMEJ synthesis substrate | taagcgatgctctcaccgagggacgtatctgctgggttgtggataccgaggcagagctgtatgtcct atcacgatcgatggtcaaaagaaggagtactccgaaggtgaggatcttcactctcacacccatc |

| | |
|---|---|
| 70 bp TMEJ synthesis substrate | taagcgatgctctcaccgagggacgtatctgctgggttgtggatgaattcatgctgtgggttgtggat cgagtagggcagagctgtatgtcctatcacgatcgatggtcaaaagaaggagtactccgaaggt gaggatcttcactctcacacccatc |
| LBR signature locus | cagtgaacacctctgcatgagcaggggcataaaaacggacgatcgtgataggacatacagctct gctttcaacatttagctcagagcctccaagtacaaagaaagaggaaggaaatgtaccctccttctc tcttctc |
| LBR upstream reference | caaaacagagcaggggagagaaagggacctgaaggcttctctcagcagaagacagacgata cttctcagccgagctgcgacgtttgggggtaagttctccaggcaaaggc |

**Figure legends**

**Fig. 1 TMEJ requires a flap-trimming exonuclease and a secondary DNA polymerase (a)** TMEJ extrachromosomal reporter system and required repair steps. TMEJ is measured by qPCR, and is initiated by annealing of microhomologies (MH, red) between the head of one DNA molecule and the tail of another. Putative Pol θ independent steps are highlighted in blue and yellow. (**b**) Quantification of extrachromosomal TMEJ in RPE1 cells with a 4 bp MH (red bars), varying phosphorothioates locations in the DNA substrate as noted (stop signs). Data is from 3 biological replicates analyzed with a one-way ANOVA and Dunnet's method. Bars represent mean and standard deviation (SD), nd; below limit of detection. (**c**) Pol θ synthesis reporter substrate. Triplicate Thymines are spaced every 8 bps along the ssDNA tract to be synthesized. (**d**) Frequencies of mutations generated by cellular TMEJ-associated synthesis (squares) vs. control synthesis (Q5 polymerase, circles) are plotted as a function of distance from the microhomology, using data from 3 biological replicates; bars represent mean and SD (**e**) Schematic of the TMEJ strand displacement reporter. Substrates have ends with partly complementary 3' overhangs that are either 4 (NHEJ) or 45 nts long (TMEJ) and possess a 5' terminal nt (dN) or abasic site (Ab.). A mismatched BamHI site is 20 or 50 bp downstream of the 5' terminus, such that repair products become sensitive to BamHI if strand displacement synthesis occurs, and remain BamHI resistant in the absence of strand displacement synthesis. (**f**) The BamHI substrates were introduced into mouse embryonic fibroblasts and digested with BamHI where indicated prior to amplification.

**Fig. 2 Polymerase Delta is both the exonuclease and secondary polymerase required for TMEJ** (**a**) *In vitro* flap cleavage experiment. 50nM double stranded DNA substrates with 2,5, and 10 nt 3' ssDNA overhangs were incubated with 50nM purified wild type (wt) or exonuclease defective Pol δ for 1 (wt) or 5 minutes (Exo mutant). (**b**) Western blot showing lentiviral shPOLD1 depletion, and expression of retroviral FLAG-tagged POLD1 constructs in the RPE1 human cell line. Actin was used as a loading control. (**c**) Quantification of repair of the 5 bp flapped substrate relative to the minimal substrate, normalized to WT. Pol θ is inhibited (Pol θi) by ART558 treatment. POLD1 in RPE1 cells is endogenously expressed (+) or depleted (-) by shPOLD1 treatment. Data is from 3 biological replicates and analyzed with a one-way ANOVA and Dunnet's

method. Bars represent data means and SDs, nd; below limit of detection. (**d**) Quantification of repair of the 70 nt synthesis substrate relative to the minimal substrate, normalized to WT. Data is from 3 biological replicates analyzed with a one-way ANOVA and Dunnet's method. Bars represent data means and SDs, nd; below limit of detection.

**Fig. 3 Polymerases Delta and Theta are equally required for chromosomal TMEJ**. (**a**) Diagram of Cas9 chromosomal repair reporter system at the LBR locus. Differences in repair are measured for NHEJ by quantification of a single nucleotide insertion, and for TMEJ by quantification of two different products mediated by microhomologies (MH), or products with templated insertions (TINS). (**b**) Quantification of TMEJ at an embedded MH by qPCR. RPE1 cells express Pol θ (+) or are genetically deficient (-). POLD1 in RPE1 cells is endogenously expressed (+) or depleted (-) by shPOLD1 treatment. Data is from 3 biological replicates analyzed with a one-way ANOVA and Dunnet's method. Bars represent data means and SDs. (**c**) Quantification of TMEJ at a terminal MH performed as in (b). (**d**) Frequency of TINS repair products as measured by digital droplet PCR. Data is from 3 biological replicates analyzed with a one-way ANOVA and Dunnet's method. Bars represent data means and SDs. (**e**) NHEJ repair quantification performed as in (b), with the exception of 2 replicates for the shPOLD1 sample.

**Fig. 4 Polymerases Delta and Theta physically associate**.
(**a**) Extracts of RPE1 cells expressing Halo-Pol θ were immunoprecipitated with an antibody to its Halo tag (αHalo) or with antibody omitted (-), and recovered proteins probed with an antibody to POLD1 (αPOLD1). Cells were untreated (-) or treated with neocarzinostatin (+NCS). **(b)** Co-IP of FLAG-tagged domains of Pol θ in POLQ$^{-/-}$ U2OS cells. Pol δ was pulled down with an antibody to POLD1, and recovered proteins probed with a FLAG antibody. Negative controls include parallel experiments using cells not expressing FLAG tagged constructs or using cells expressing FLAG-tagged constructs but with αPOLD1 omitted (**c**) Representative STORM reconstructed image of 53BP1, Halo-Pol θ, and POLD1 in a single nucleus. White boxes denote triple association events. Scale bar is 150 nm. (**d**) Quantification of STORM in (c). Density of POLD1 at sites of Pol θ-53BP1 localization was plotted with and without NCS pre-treatment. Data is from 3 biological replicates analyzed with a paired t-test. (**e**) Model of polymerases Delta and Theta's cooperation in TMEJ. DSBs containing a MH are identified by Theta and MHs are aligned and annealed together by Theta's helicase-like domain. Polymerase Delta's exonuclease domain cleaves resulting DNA flaps from non-terminal MH alignments. Theta initiates DNA synthesis from the MH site and hands over DNA synthesis to Delta within approximately ~10 bps.

**Extended data fig. 1 Strand displacement in TMEJ** (**a**) Schematic of mismatched BamHI substrate design to measure strand displacement of 20 and 50 bps in TMEJ. (**b**) Gel of DNA substrates in (a) with BamHI sensitive and resistant TMEJ repair products. (**c**) Quantification of strand displacement (BamHI sensitivity) 20 bp or 50 bp into double stranded DNA. The mean fraction of strand displacement was determined for three independent experiments. Error bars denote the standard error of the mean.

**Extended data fig. 2 Polymerase Delta is both the exonuclease and secondary polymerase required for TMEJ** (**a**) *In vitro* flap cleavage experiment. 50 nM double stranded DNA substrate with a 5 nt 3' ssDNA overhang and phosphorothioates at the most terminal 3' positions was incubated with purified wt Pol δ for 1 minute. (**b**) Schematic of viral timeline for transfection and transduction to generate cell lines. (**c**) Schematic of the nuclease-dependent TMEJ substrate (blue box), the synthesis-dependent substrate (yellow box), and the minimal TMEJ substrate reporter (grey box). (**d**) Quantification of repair of a 2 bp flapped substrate relative to the minimal TMEJ substrate, normalized to WT. Data is from 3 biological replicates analyzed with a one-way ANOVA and Dunnett's method. Bars represent data means and SDs, nd; below limit of detection. (**e**) 10 bp flapped substrate performed as in (c). (**f**) Quantification of repair of a 45 bp synthesis substrate relative to the minimal TMEJ substrate, normalized to WT. Data is from 3 biological replicates analyzed with a one-way ANOVA and Dunnet's method. Bars represent data means and SDs.

**Extended data fig. 3 TMEJ qPCR detection validation** (**a**) Quantification of unflapped and flapped TMEJ repair normalized to NHEJ with and without Pol θi (ART558). Data is from 3 biological replicates. Bars represent data mean and SD. (**b**) Standard curve of qPCR CT values of a unflapped and flapped TMEJ model product where the amount of flapped product is constant and unflapped is varied. (**c**) Identical to (b), but flapped is varied and unflapped is constant. (**d**) Standard curve of qPCR CT values of a 45 bp and 25 bp TMEJ synthesis model products where the 25 bp product is constant and the 45 bp product is varied. (**e**) Identical to (d), but the 45 bp product is varied and the 25 bp product is constant. (**f**) Standard curve of qPCR CT values of a 70 bp and 25 bp TMEJ synthesis model products where the 25 bp product is constant and the 70 bp product is varied. (**g**) Identical to (f), but the 25 bp product is varied and the 70 bp product is constant. (**h**) Standard curve of qPCR CT values of the LBR repair signature and reference model products where the signature product is varied and the reference product is constant. (**i**) Identical to (h), but the reference product is varied and the signature product is constant.

**Extended data fig. 4 Chromosomal LBR reporter characterization and controls** (**a**) Predicted microhomology-mediated deletion repair products at the LBR locus. (**b**) Sequence alignments of predicted microhomology-mediated deletion repair intermediates. (**c**) Western blot of shPOLE treated RPE1 cells and an untreated control. Actin was used as a loading control. (**d**) Quantification of the terminal TMEJ repair product at LBR relative to the signature NHEJ product for WT, shPOLD1, and shPOLE treated RPE1 cells. Bars represent data mean and SD.

**Extended data fig. 5 Uncropped gels and western blots** (**a**) Western blot from data fig. 2b displaying Actin (red), POLD1 (green), and FLAG (yellow). (**b**) Western blot from extended data fig. 4a. Top blot displays POLD1 (green) and FLAG (dual color). Bottom blot displays Actin (blue). (**c**) Co-IP of fig. 4c displaying POLD1. (**d**) Co-IP of fig. 4d displaying FLAG. (**e**) Gel from data fig. 2a. (**f**) Gel from extended data fig. 2b. (**g**) Western blot from extended data fig 4b.

## References


1 Ramsden, D. A., Carvajal-Garcia, J. & Gupta, G. P. Mechanism, cellular functions and cancer roles of polymerase-theta-mediated DNA end joining. *Nat Rev Mol Cell Biol*, doi:10.1038/s41580-021-00405-2 (2021).

2 Minocherhomji, S. *et al.* Replication stress activates DNA repair synthesis in mitosis. *Nature* **528**, 286-290, doi:10.1038/nature16139 (2015).

3 Costantino, L. *et al.* Break-induced replication repair of damaged forks induces genomic duplications in human cells. *Science* **343**, 88-91, doi:10.1126/science.1243211 (2014).

4 Kent, T., Chandramouly, G., McDevitt, S. M., Ozdemir, A. Y. & Pomerantz, R. T. Mechanism of microhomology-mediated end-joining promoted by human DNA polymerase theta. *Nat Struct Mol Biol* **22**, 230-237, doi:10.1038/nsmb.2961 (2015).

5 Wyatt, D. W. *et al.* Essential Roles for Polymerase theta-Mediated End Joining in the Repair of Chromosome Breaks. *Mol Cell* **63**, 662-673, doi:10.1016/j.molcel.2016.06.020 (2016).

6 Yousefzadeh, M. J. *et al.* Mechanism of suppression of chromosomal instability by DNA polymerase POLQ. *PLoS Genet* **10**, e1004654, doi:10.1371/journal.pgen.1004654 (2014).

7 Carvajal-Garcia, J. *et al.* Mechanistic basis for microhomology identification and genome scarring by polymerase theta. *Proc Natl Acad Sci U S A* **117**, 8476-8485, doi:10.1073/pnas.1921791117 (2020).

8 Eckstein, F. Nucleoside phosphorothioates. *Annu Rev Biochem* **54**, 367-402, doi:10.1146/annurev.bi.54.070185.002055 (1985).

9 Arana, M. E., Seki, M., Wood, R. D., Rogozin, I. B. & Kunkel, T. A. Low-fidelity DNA synthesis by human DNA polymerase theta. *Nucleic Acids Res* **36**, 3847-3856, doi:10.1093/nar/gkn310 (2008).

10 Schmitt, M. W. *et al.* Active site mutations in mammalian DNA polymerase delta alter accuracy and replication fork progression. *J Biol Chem* **285**, 32264-32272, doi:10.1074/jbc.M110.147017 (2010).

11 Weedon, M. N. *et al.* An in-frame deletion at the polymerase active site of POLD1 causes a multisystem disorder with lipodystrophy. *Nat Genet* **45**, 947-950, doi:10.1038/ng.2670 (2013).

12 Schimmel, J., van Schendel, R., den Dunnen, J. T. & Tijsterman, M. Templated Insertions: A Smoking Gun for Polymerase Theta-Mediated End Joining. *Trends Genet* **35**, 632-644, doi:10.1016/j.tig.2019.06.001 (2019).

13 Feng, W. *et al.* Marker-free quantification of repair pathway utilization at Cas9-induced double-strand breaks. *Nucleic Acids Res* **49**, 5095-5105, doi:10.1093/nar/gkab299 (2021).

14 Lee, K. & Lee, S. E. Saccharomyces cerevisiae Sae2- and Tel1-dependent single-strand DNA formation at DNA break promotes microhomology-mediated end joining. *Genetics* **176**, 2003-2014, doi:10.1534/genetics.107.076539 (2007).

15 Meyer, D., Fu, B. X. & Heyer, W. D. DNA polymerases delta and lambda cooperate in repairing double-strand breaks by microhomology-mediated end-

joining in Saccharomyces cerevisiae. *Proc Natl Acad Sci U S A* **112**, E6907-6916, doi:10.1073/pnas.1507833112 (2015).
16 Villarreal, D. D. *et al.* Microhomology directs diverse DNA break repair pathways and chromosomal translocations. *PLoS Genet* **8**, e1003026, doi:10.1371/journal.pgen.1003026 (2012).
17 Takata, K. I. *et al.* Analysis of DNA polymerase nu function in meiotic recombination, immunoglobulin class-switching, and DNA damage tolerance. *PLoS Genet* **13**, e1006818, doi:10.1371/journal.pgen.1006818 (2017).
18 Simon, M., Giot, L. & Faye, G. The 3' to 5' exonuclease activity located in the DNA polymerase delta subunit of Saccharomyces cerevisiae is required for accurate replication. *EMBO J* **10**, 2165-2170, doi:10.1002/j.1460-2075.1991.tb07751.x (1991).
19 Paques, F. & Haber, J. E. Two pathways for removal of nonhomologous DNA ends during double-strand break repair in Saccharomyces cerevisiae. *Mol Cell Biol* **17**, 6765-6771, doi:10.1128/MCB.17.11.6765 (1997).
20 Ulrich, H. D. & Walden, H. Ubiquitin signalling in DNA replication and repair. *Nat Rev Mol Cell Biol* **11**, 479-489, doi:10.1038/nrm2921 (2010).
21 Burgers, P. M. J. & Kunkel, T. A. Eukaryotic DNA Replication Fork. *Annu Rev Biochem* **86**, 417-438, doi:10.1146/annurev-biochem-061516-044709 (2017).
22 He, P. & Yang, W. Template and primer requirements for DNA Pol theta-mediated end joining. *Proc Natl Acad Sci U S A* **115**, 7747-7752, doi:10.1073/pnas.1807329115 (2018).
23 Mengwasser, K. E. *et al.* Genetic Screens Reveal FEN1 and APEX2 as BRCA2 Synthetic Lethal Targets. *Mol Cell* **73**, 885-899 e886, doi:10.1016/j.molcel.2018.12.008 (2019).
24 Boboila, C. *et al.* Robust chromosomal DNA repair via alternative end-joining in the absence of X-ray repair cross-complementing protein 1 (XRCC1). *Proc Natl Acad Sci U S A* **109**, 2473-2478, doi:10.1073/pnas.1121470109 (2012).
25 Masani, S., Han, L., Meek, K. & Yu, K. Redundant function of DNA ligase 1 and 3 in alternative end-joining during immunoglobulin class switch recombination. *Proc Natl Acad Sci U S A* **113**, 1261-1266, doi:10.1073/pnas.1521630113 (2016).
26 Mateos-Gomez, P. A. *et al.* Mammalian polymerase theta promotes alternative NHEJ and suppresses recombination. *Nature* **518**, 254-257, doi:10.1038/nature14157 (2015).
27 Simsek, D. *et al.* DNA ligase III promotes alternative nonhomologous end-joining during chromosomal translocation formation. *PLoS Genet* **7**, e1002080, doi:10.1371/journal.pgen.1002080 (2011).
28 Almeida, K. H. & Sobol, R. W. A unified view of base excision repair: lesion-dependent protein complexes regulated by post-translational modification. *DNA Repair (Amst)* **6**, 695-711, doi:10.1016/j.dnarep.2007.01.009 (2007).
29 Kao, H. I. & Bambara, R. A. The protein components and mechanism of eukaryotic Okazaki fragment maturation. *Crit Rev Biochem Mol Biol* **38**, 433-452, doi:10.1080/10409230390259382 (2003).
30 Feng, W. *et al.* Genetic determinants of cellular addiction to DNA polymerase theta. *Nat Commun* **10**, 4286, doi:10.1038/s41467-019-12234-1 (2019).

31 Llorens-Agost, M. *et al.* POLtheta-mediated end joining is restricted by RAD52 and BRCA2 until the onset of mitosis. *Nat Cell Biol* **23**, 1095-1104, doi:10.1038/s41556-021-00764-0 (2021).
32 Roerink, S. F., van Schendel, R. & Tijsterman, M. Polymerase theta-mediated end joining of replication-associated DNA breaks in C. elegans. *Genome Res* **24**, 954-962, doi:10.1101/gr.170431.113 (2014).
33 van Schendel, R., Romeijn, R., Buijs, H. & Tijsterman, M. Preservation of lagging strand integrity at sites of stalled replication by Pol alpha-primase and 9-1-1 complex. *Sci Adv* **7**, doi:10.1126/sciadv.abf2278 (2021).
34 Wang, Z. *et al.* DNA polymerase theta (POLQ) is important for repair of DNA double-strand breaks caused by fork collapse. *J Biol Chem* **294**, 3909-3919, doi:10.1074/jbc.RA118.005188 (2019).
35 Deshpande, M. *et al.* Error-prone repair of stalled replication forks drives mutagenesis and loss of heterozygosity in haploinsufficient BRCA1 cells. *Molecular Cell*, doi:https://doi.org/10.1016/j.molcel.2022.08.017 (2022).
36 Donnianni, R. A. *et al.* DNA Polymerase Delta Synthesizes Both Strands during Break-Induced Replication. *Mol Cell* **76**, 371-381 e374, doi:10.1016/j.molcel.2019.07.033 (2019).
37 Layer, J. V. *et al.* Polymerase delta promotes chromosomal rearrangements and imprecise double-strand break repair. *Proc Natl Acad Sci U S A* **117**, 27566-27577, doi:10.1073/pnas.2014176117 (2020).
38 Luedeman, M. E. *et al.* Poly(ADP) ribose polymerase promotes DNA polymerase theta-mediated end joining by activation of end resection. *Nat Commun* **13**, 4547, doi:10.1038/s41467-022-32166-7 (2022).
39 Hwang, T. *et al.* Defining the mutation signatures of DNA polymerase theta in cancer genomes. *NAR Cancer* **2**, zcaa017, doi:10.1093/narcan/zcaa017 (2020).
40 Kiktev, D. A. *et al.* The fidelity of DNA replication, particularly on GC-rich templates, is reduced by defects of the Fe-S cluster in DNA polymerase delta. *Nucleic Acids Res* **49**, 5623-5636, doi:10.1093/nar/gkab371 (2021).
41 Holden, S. J., Uphoff, S. & Kapanidis, A. N. DAOSTORM: an algorithm for high-density super-resolution microscopy. *Nat Methods* **8**, 279-280, doi:10.1038/nmeth0411-279 (2011).
42 Huang, F. *et al.* Video-rate nanoscopy using sCMOS camera-specific single-molecule localization algorithms. *Nat Methods* **10**, 653-658, doi:10.1038/nmeth.2488 (2013).
43 Huang, F., Schwartz, S. L., Byars, J. M. & Lidke, K. A. Simultaneous multiple-emitter fitting for single molecule super-resolution imaging. *Biomed Opt Express* **2**, 1377-1393, doi:10.1364/BOE.2.001377 (2011).
44 Yin, Y., Lee, W. T. C. & Rothenberg, E. Ultrafast data mining of molecular assemblies in multiplexed high-density super-resolution images. *Nat Commun* **10**, 119, doi:10.1038/s41467-018-08048-2 (2019).
45 Sengupta, P. *et al.* Probing protein heterogeneity in the plasma membrane using PALM and pair correlation analysis. *Nat Methods* **8**, 969-975, doi:10.1038/nmeth.1704 (2011).

765 46 Veatch, S. L. *et al.* Correlation functions quantify super-resolution images and
766 estimate apparent clustering due to over-counting. *PLoS One* **7**, e31457,
767 doi:10.1371/journal.pone.0031457 (2012).
768
769

Fig. 1

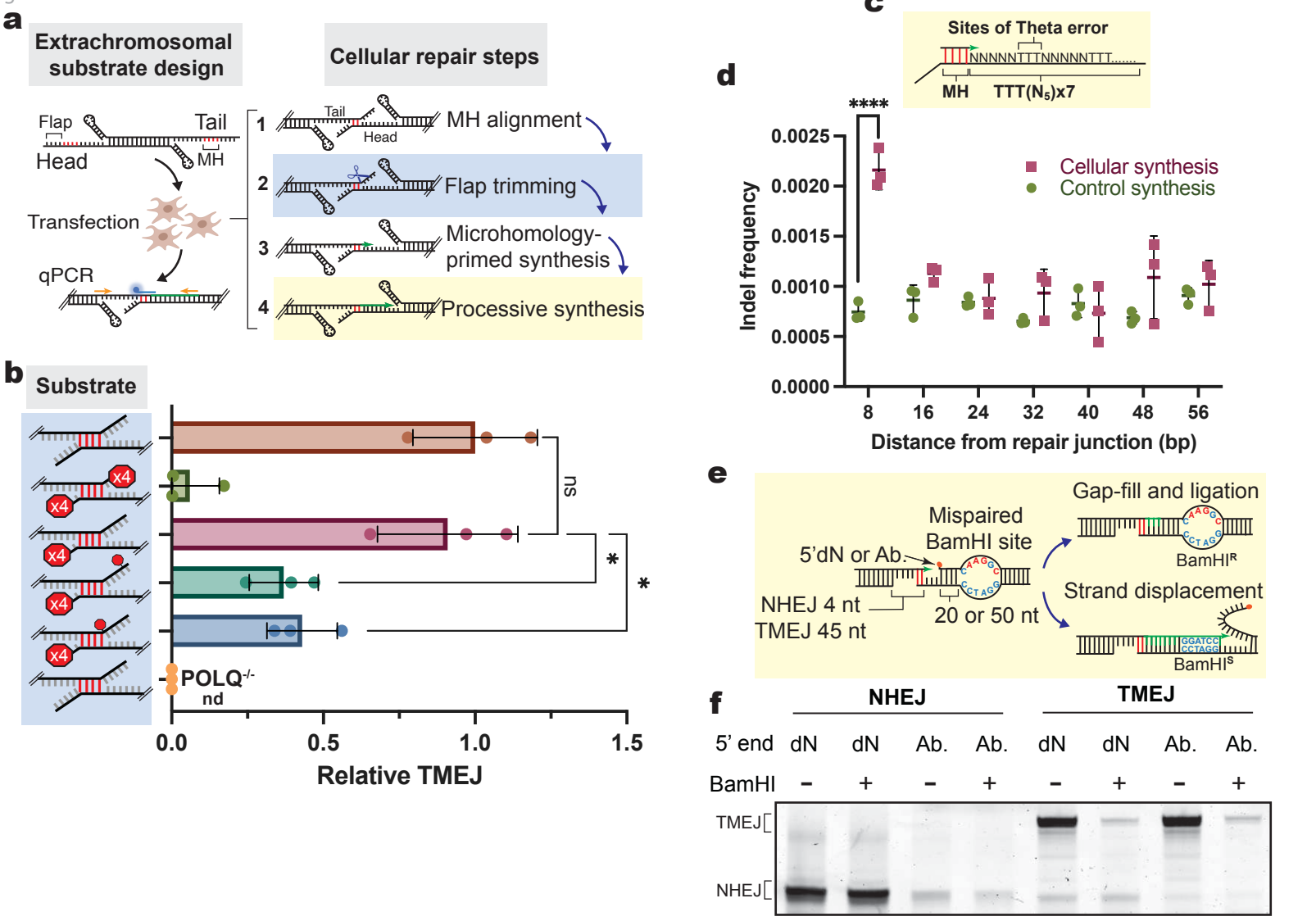


**Fig. 1 TMEJ requires a flap-trimming exonuclease and a secondary DNA polymerase** (a) TMEJ extrachromosomal reporter system and required repair steps. TMEJ is measured by qPCR, and is initiated by annealing of microhomologies (MH, red) between the head of one DNA molecule and the tail of another. Putative Pol θ independent steps are highlighted in blue and yellow. (b) Quantification of extrachromosomal TMEJ in RPE1 cells with a 4 bp MH (red bars), varying phosphorothioates locations in the DNA substrate as noted (stop signs). Data is from 3 biological replicates analyzed with a one-way ANOVA and Dunnet's method. Bars represent mean and standard deviation (SD), nd; below limit of detection. (c) Pol θ synthesis reporter substrate. Triplicate Thymines are spaced every 8 bps along the ssDNA tract to be synthesized. (d) Frequencies of mutations generated by cellular TMEJ-associated synthesis (squares) vs. control synthesis (Q5 polymerase, circles) are plotted as a function of distance from the microhomology, using data from 3 biological replicates; bars represent mean and SD (e) Schematic of the TMEJ strand displacement reporter. Substrates have ends with partly complementary 3' overhangs that are either 4 (NHEJ) or 45 nts long (TMEJ) and possess a 5' terminal nt (dN) or abasic site (Ab.). A mismatched BamHI site is 20 or 50 bp downstream of the 5' terminus, such that repair products become sensitive to BamHI if strand displacement synthesis occurs, and remain BamHI resistant in the absence of strand displacement synthesis. (f) The BamHI substrates were introduced into mouse embryonic fibroblasts and digested with BamHI where indicated prior to amplification.

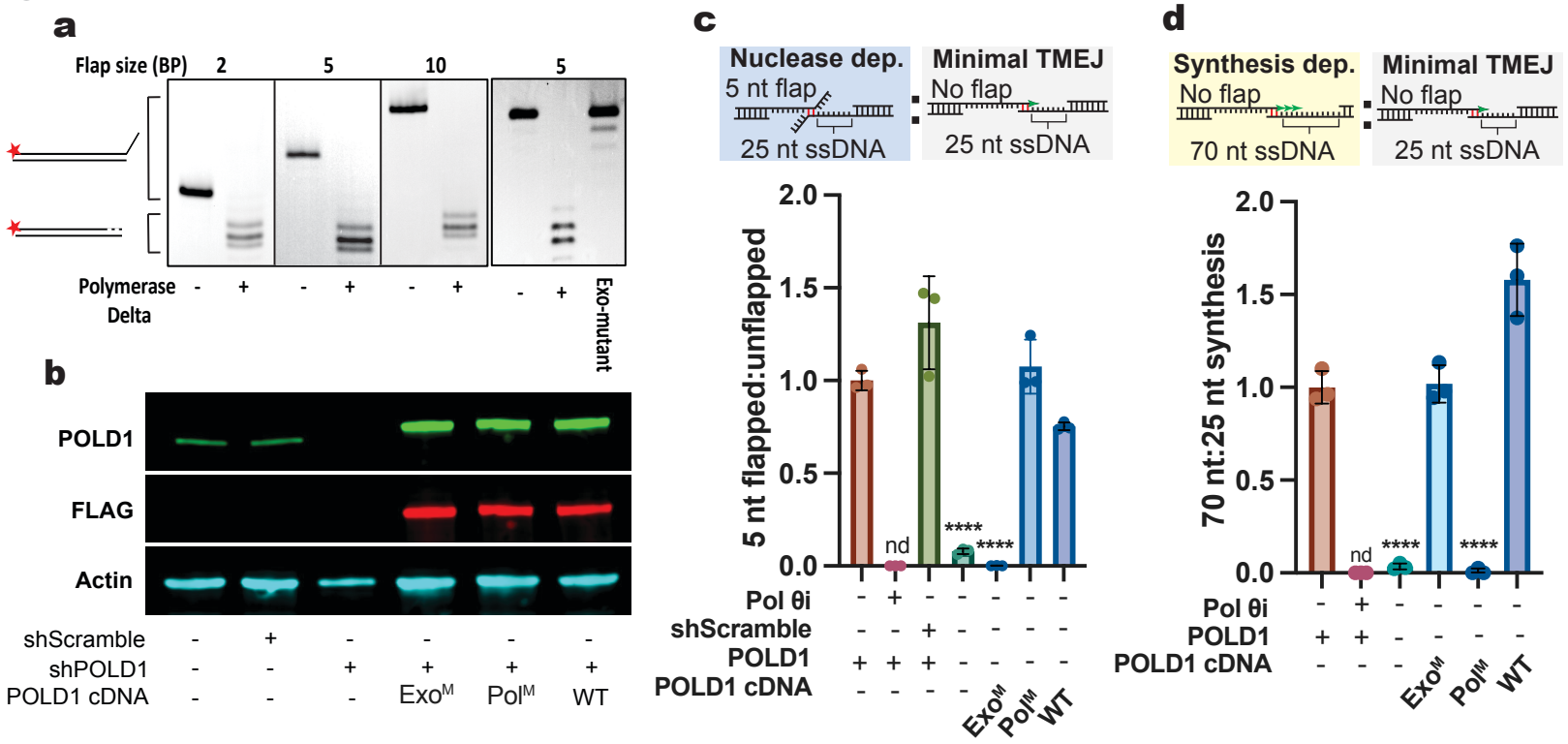


**Fig. 2 Polymerase Delta is both the exonuclease and secondary polymerase required for TMEJ** (a) In vitro flap cleavage experiment. 50nM double stranded DNA substrates with 2,5, and 10 nt 3' ssDNA overhangs were incubated with 50nM purified wild type (wt) or exonuclease defective Pol δ for 1 (wt) or 5 minutes (Exo mutant). (b) Western blot showing lentiviral shPOLD1 depletion, and expression of retroviral FLAG-tagged POLD1 constructs in the RPE1 human cell line. Actin was used as a loading control. (c) Quantification of repair of the 5 bp flapped substrate relative to the minimal substrate, normalized to WT. Pol θ is inhibited (Pol θi) by ART558 treatment. POLD1 in RPE1 cells is endogenously expressed (+) or depleted (-) by shPOLD1 treatment. Data is from 3 biological replicates and analyzed with a one-way ANOVA and Dunnet's method. Bars represent data means and SDs, nd; below limit of detection. (d) Quantification of repair of the 70 nt synthesis substrate relative to the minimal substrate, normalized to WT. Data is from 3 biological replicates analyzed with a one-way ANOVA and Dunnet's method. Bars represent data means and SDs, nd; below limit of detection..

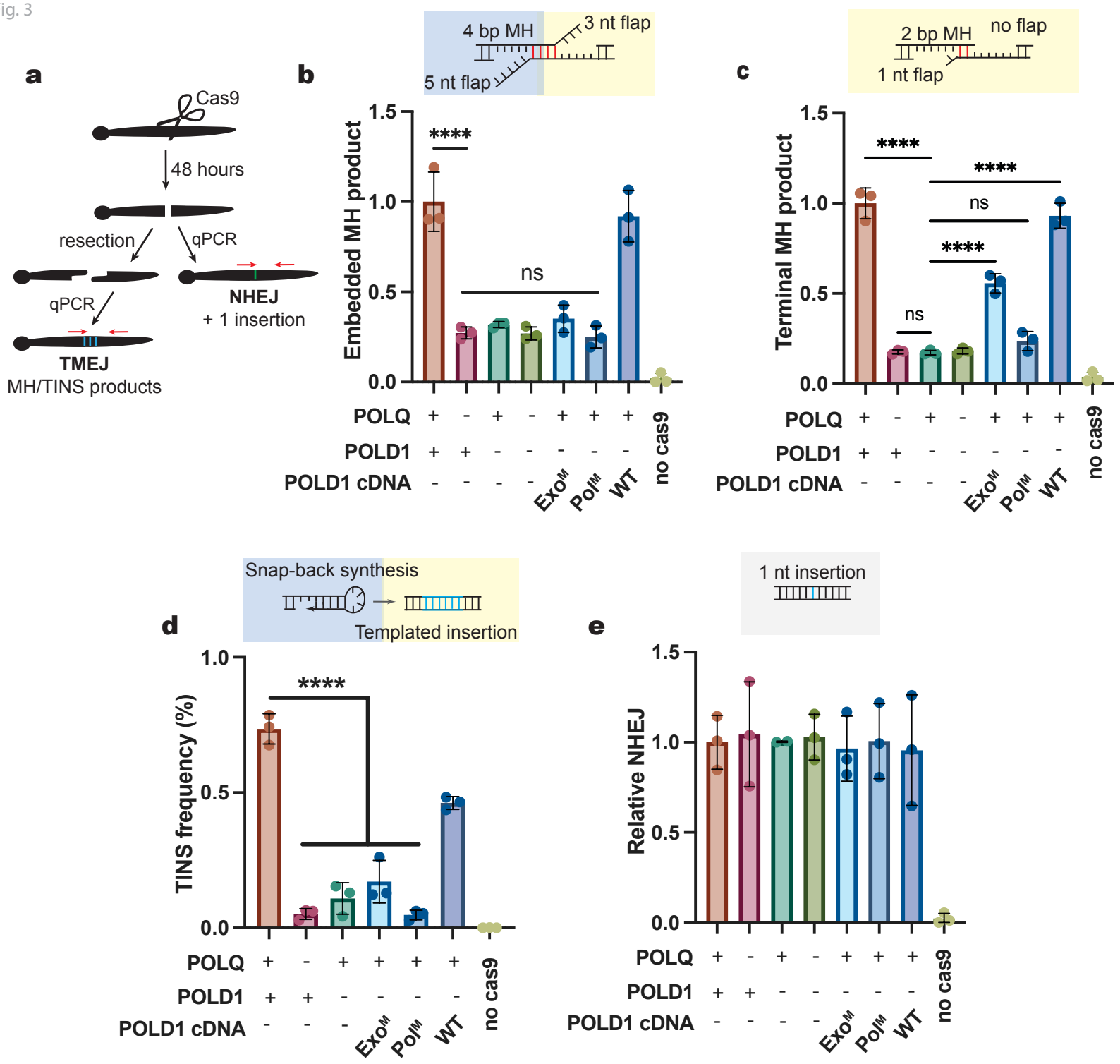


**Fig. 3 Polymerases Delta and Theta are equally required for chromosomal TMEJ** (a) Diagram of Cas9 chromosomal repair reporter system at the LBR locus. Differences in repair are measured for NHEJ by quantification of a single nucleotide insertion, and for TMEJ by quantification of two different products mediated by microhomologies (MH), or products with templated insertions (TINS). (b) Quantification of TMEJ at an embedded MH by qPCR. RPE1 cells express Pol θ (+) or are genetically deficient (-). POLD1 in RPE1 cells is endogenously expressed (+) or depleted (-) by shPOLD1 treatment. Data is from 3 biological replicates analyzed with a one-way ANOVA and Dunnet's method. Bars represent data means and SDs. (c) Quantification of TMEJ at a terminal MH performed as in (b). (d) Frequency of TINS repair products as measured by digital droplet PCR. Data is from 3 biological replicates analyzed with a one-way ANOVA and Dunnet's method. Bars represent data means and SDs. (e) NHEJ repair quantification performed as in (b), with the exception of 2 replicates for the shPOLD1 sample.

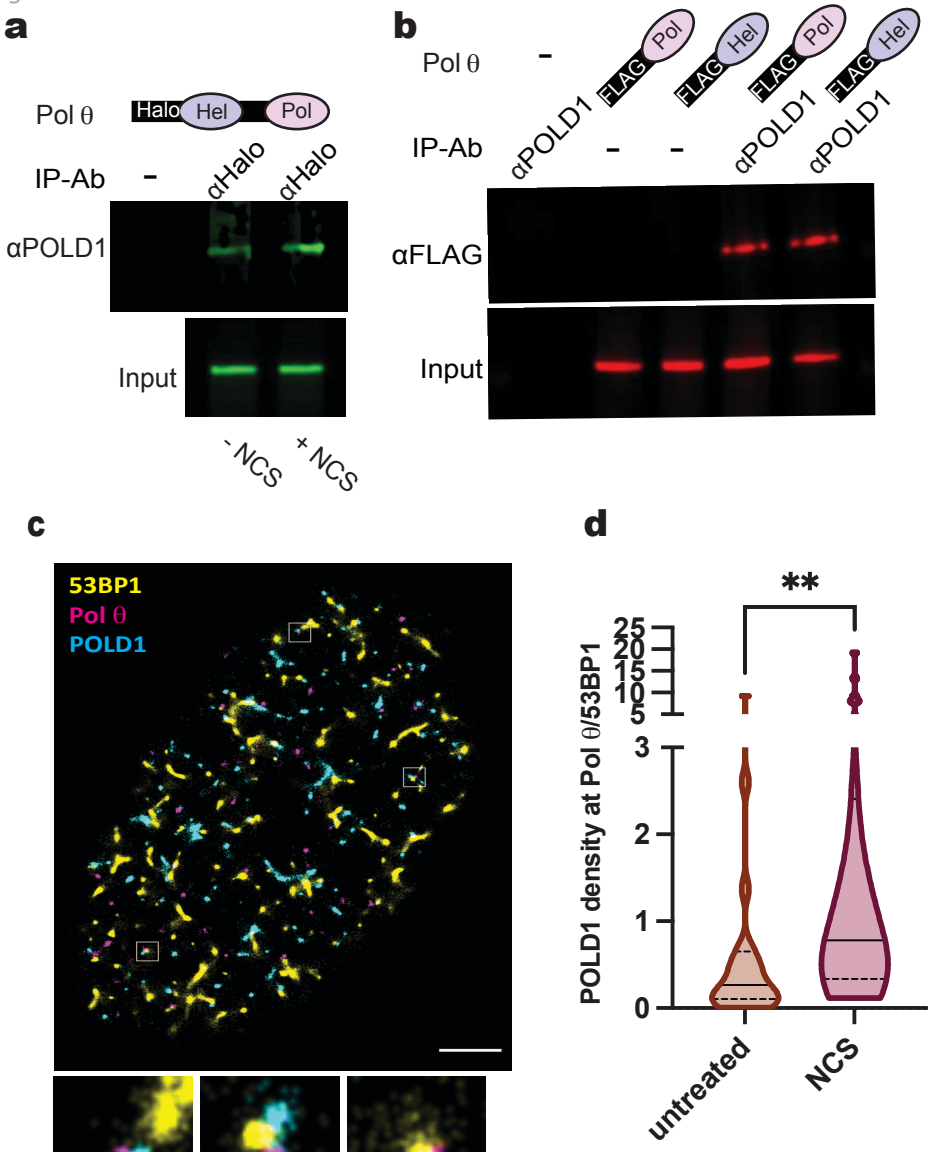








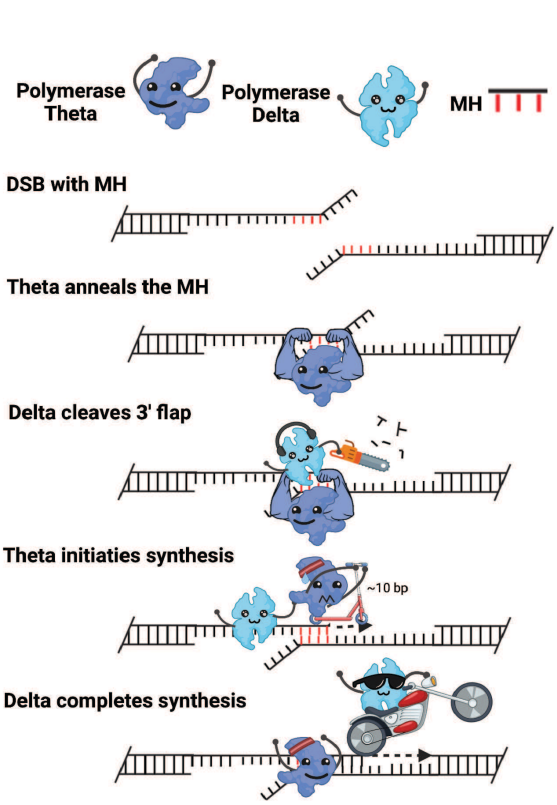


**Fig. 4 Polymerases Delta and Theta physically associate.** (a) Extracts of RPE1 cells expressing Halo-Pol θ were immunoprecipitated with an antibody to its Halo tag (αHalo) or with antibody omitted (-), and recovered proteins probed with an antibody to POLD1 (αPOLD1). Cells were untreated (-) or treated with neocarzinostatin (+NCS). (b) Co-IP of FLAG-tagged domains of Pol θ in POLQ-/- U2OS cells. Pol δ was pulled down with an antibody to POLD1, and recovered proteins probed with a FLAG antibody. Negative controls include parallel experiments using cells not expressing FLAG-tagged constructs or using cells expressing FLAG-tagged constructs but with αPOLD1 omitted (c) Representative STORM reconstructed image of 53BP1, Halo-Pol θ, and POLD1 in a single nucleus. White boxes denote triple association events. Scale bar is 150 nm. (d) Quantification of STORM in (c). Density of POLD1 at sites of Pol θ-53BP1 localization was plotted with and without NCS pre-treatment. Data is from 3 biological replicates analyzed with a paired t-test. (e) Model of polymerases Delta and Theta's cooperation in TMEJ. DSBs containing a MH are identified by Theta and MHs are aligned and annealed together by Theta's helicase-like domain. Polymerase Delta's exonuclease domain cleaves resulting DNA flaps from non-terminal MH alignments. Theta initiates DNA synthesis from the MH site and hands over DNA synthesis to Delta within approximately ~10 bps.

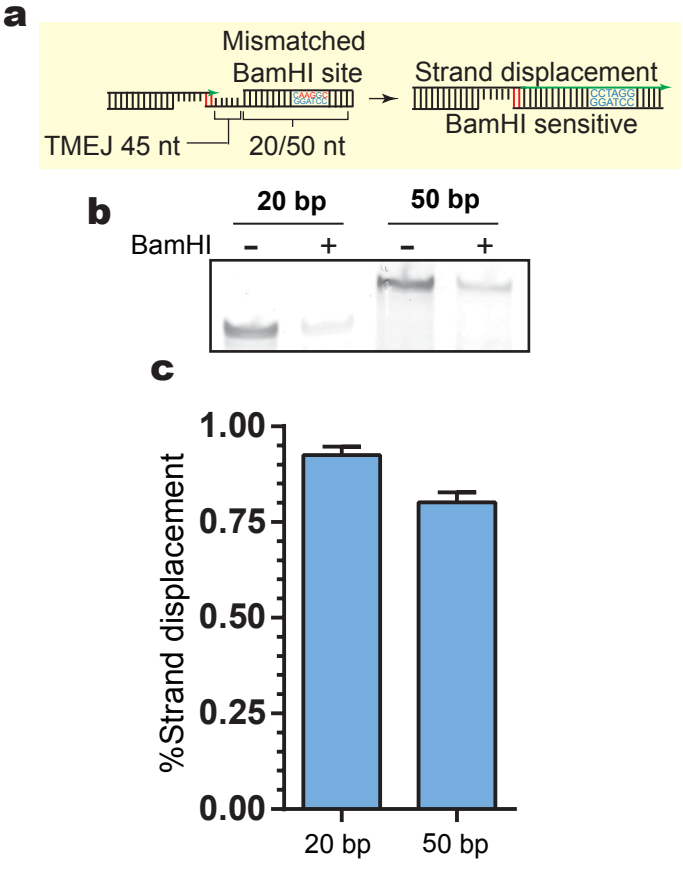


**Extended data fig. 1 Strand displacement in TMEJ** (a) Schematic of mismatched BamHI substrate design to measure strand displacement of 20 and 50 bps in TMEJ. (b) Gel of DNA substrates in (a) with BamHI sensitive and resistant TMEJ repair products. (c) Quantification of strand displacement (BamHI sensitivity) 20 bp or 50 bp into double stranded DNA. The mean fraction of strand displacement was determined for three independent experiments. Error bars denote the standard error of the mean..

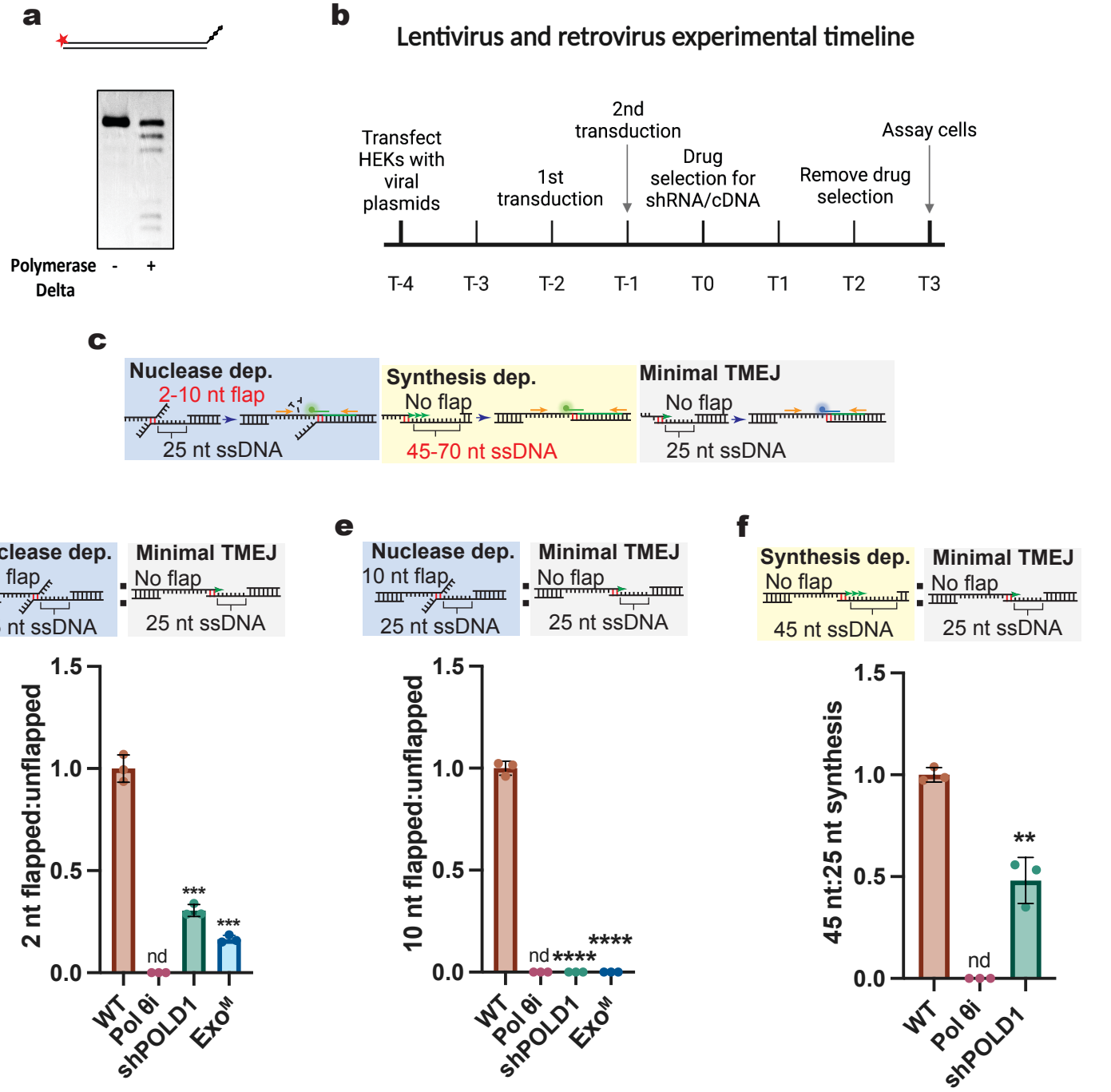


**Extended data fig. 2 Polymerase Delta is both the exonuclease and secondary polymerase required for TMEJ** (a) In vitro flap cleavage experiment. 50 nM double stranded DNA substrate with a 5 nt 3' ssDNA overhang and phosphorothioates at the most terminal 3' positions was incubated with purified wt Pol δ for 1 minute. (b) Schematic of viral timeline for transfection and transduction to generate cell lines. (c) Schematic of the nuclease-dependent TMEJ substrate (blue box), the synthesis-dependent substrate (yellow box), and the minimal TMEJ substrate reporter (grey box). (d) Quantification of repair of a 2 bp flapped substrate relative to the minimal TMEJ substrate, normalized to WT. Data is from 3 biological replicates analyzed with a one-way ANOVA and Dunnett's method. Bars represent data means and SDs, nd; below limit of detection. (e) 10 bp flapped substrate performed as in (c). (f) Quantification of repair of a 45 bp synthesis substrate relative to the minimal TMEJ substrate, normalized to WT. Data is from 3 biological replicates analyzed with a one-way ANOVA and Dunnet's method. Bars represent data means and SDs.

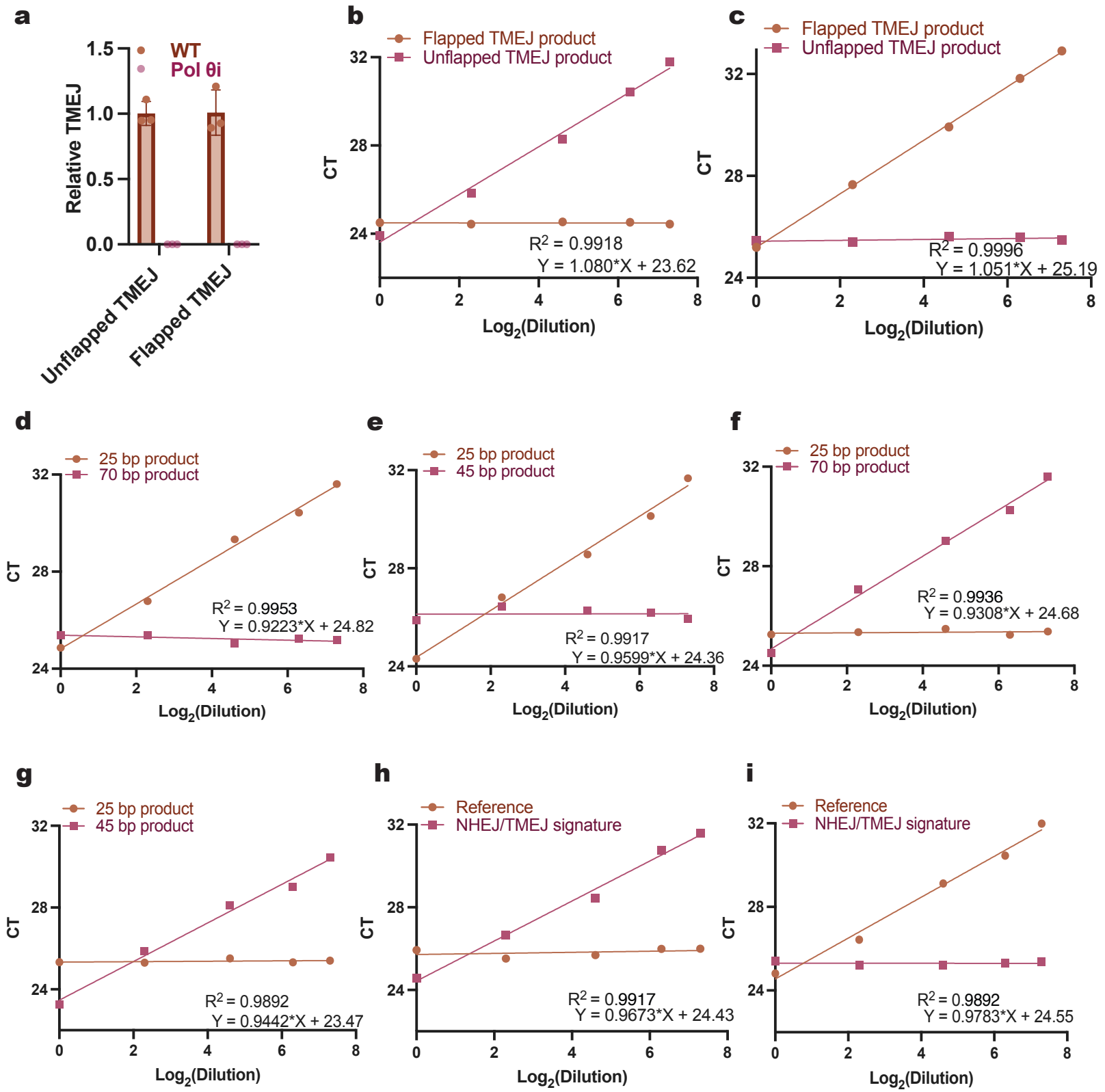


**Extended data fig. 3 TMEJ qPCR detection validation** (a) Quantification of unflapped and flapped TMEJ repair normalized to NHEJ with and without Pol θi (ART558). Data is from 3 biological replicates. Bars represent data mean and SD. (b) Standard curve of qPCR CT values of a unflapped and flapped TMEJ model product where the amount of flapped product is constant and unflapped is varied. (c) Identical to (b), but flapped is varied and unflapped is constant. (d) Standard curve of qPCR CT values of a 45 bp and 25 bp TMEJ synthesis model products where the 25 bp product is constant and the 45 bp product is varied. (e) Identical to (d), but the 45 bp product is varied and the 25 bp product is constant. (f) Standard curve of qPCR CT values of a 70 bp and 25 bp TMEJ synthesis model products where the 25 bp product is constant and the 70 bp product is varied. (g) Identical to (f), but the 25 bp product is varied and the 70 bp product is constant. (h) Standard curve of qPCR CT values of the LBR repair signature and reference model products where the signature product is varied and the reference product is constant. (i) Identical to (h), but the reference product is varied and the signature product is constant..

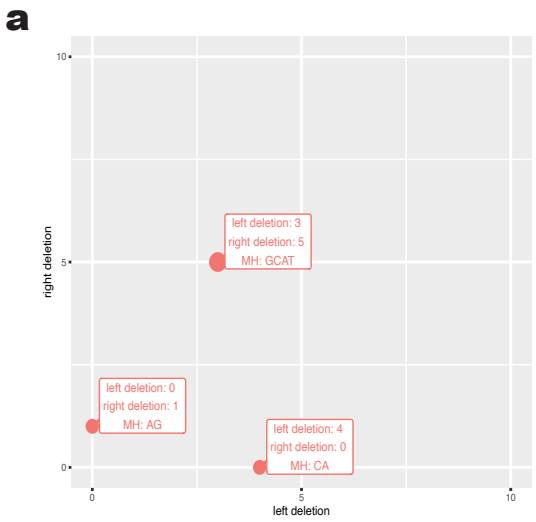


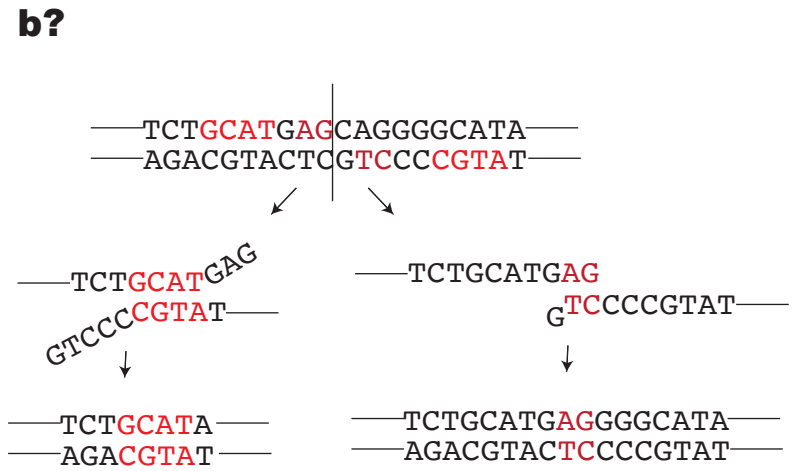


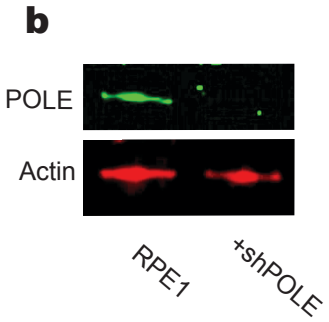


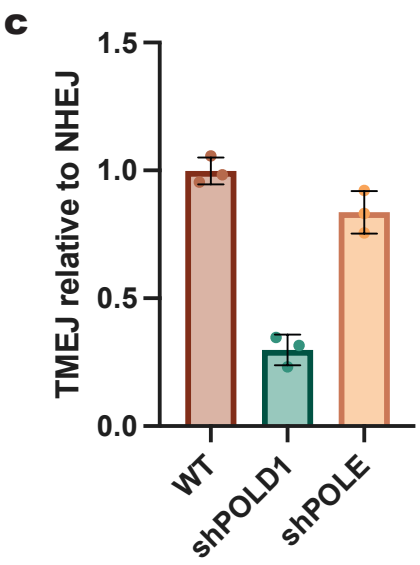


**Extended data fig. 4 Chromosomal LBR reporter characterization and controls** (a) Predicted microhomology-mediated deletion repair products at the LBR locus. (b) Sequence alignments of predicted microhomology-mediated deletion repair intermediates. (c) Western blot of shPOLE treated RPE1 cells and an untreated control. Actin was used as a loading control. (d) Quantification of the terminal TMEJ repair product at LBR relative to the signature NHEJ product for WT, shPOLD1, and shPOLE treated RPE1 cells. Bars represent data mean and SD.

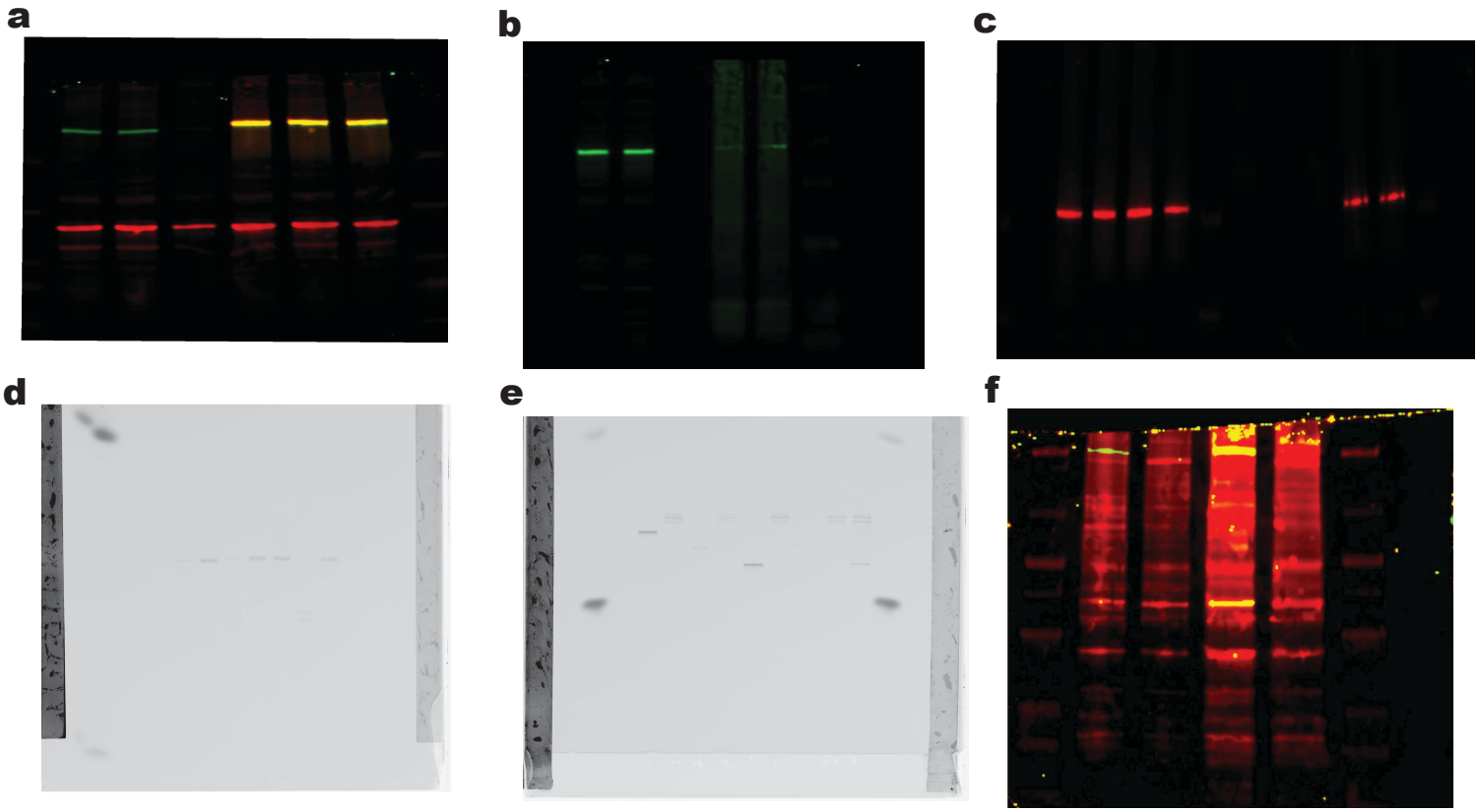


**Extended data fig. 5 Uncropped gels and western blots** (a) Western blot from data fig. 2b displaying Actin (red), POLD1 (green), and FLAG (yellow). (b) Western blot from extended data fig. 4a. Top blot displays POLD1 (green) and FLAG (dual color). Bottom blot displays Actin (blue). (c) Co-IP of fig. 4c displaying POLD1. (d) Co-IP of fig. 4d displaying FLAG. (e) Gel from data fig. 2a. (f) Gel from extended data fig. 2b. (g) Western blot from extended data fig 4b.